Ph.D. DISSERTATION

Analysis and Improvement of Internal Quantum Efficiency in GaN-based LEDs

질화갈륨 발광다이오드의 내부 양자 효율에 대한 분석 및 향상

BY

GARAM KIM

August 2014

DEPARTMENT OF ELECTRICAL AND
COMPUTER ENGINEERING
COLLEGE OF ENGINEERING
SEOUL NATIONAL UNIVERSITY

Analysis and Improvement of Internal Quantum Efficiency in GaN-based LEDs

질화갈륨 발광다이오드의 내부 양자 효율에 대한 분석 및 향상

指導敎授 朴 炳 國

이 論文을 工學博士 學位論文으로 提出함

2014 년 8 월

서울大學校 大學院

電氣·情報 工學部

김 가 람

김가람의 工學博士 學位論文을 認准함

2014 년 8 월

委 員 長 : 서 광 석 (印)

副委員長 : 박 병 국 (印)

委 員 : 이 종 호 (印)

委 員 : 박 용 조 (印)

委 員 : 조 성 재 (印)

Abstract

In order to extract the recombination coefficient and the internal quantum efficiency (IQE) of the GaN-based LEDs, a fast and reliable measurement method using transient characteristics is developed. For accurate extraction of the recombination coefficients and the IQE, an improved rate equation model for GaN-based LEDs considering the effective volume of the active region is also proposed. Through TCAD simulations, it is confirmed that the IQE, especially efficiency droop is related with small effective volume. Also, it is confirmed that the effective volume is controlled by polarization charge, the barriers between the quantum wells, and current density.

The trap and its impact on the GaN-based LEDs are also analyzed by measurement and TCAD simulation. A reversible increase in the current of GaN-based blue LEDs is observed when constant forward voltage is applied. This characteristic is assumed to be the result of trapping process, and a trap activation energy of 0.30 eV is extracted. Through TCAD simulations, it is confirmed that the multi-quantum well (MQW) barrier height is reduced by the hole trapping process and that the current is increased by lowering this barrier. It is also confirmed that the effect of this trap on the optical characteristics of GaN-based blue LEDs by TCAD simulation and measurement.

To improve the IQE of GaN-based LEDs, a novel structure for GaN-based LED featuring p-type trench in the MQW is proposed. Through TCAD simulation, it is

confirmed that the proposed structure shows quite uniform hole distribution in the MQW than that of the conventional structure, because holes are injected efficiently into the MQW along the p-type trench. It is also confirmed that the proposed structure also has a significant effect on strain relaxation and reduction in quantum confined stark effect by cathodo-luminescence (CL) measurement. In addition, two simple fabrication methods using e-beam lithography and selective wet etching for manufacturing the proposed structure are also proposed. From the measurement results of the manufactured GaN-based LEDs, it is confirmed that the proposed structure using e-beam lithography or selective wet etching shows improved light output power compared to the conventional structure because of more uniform hole distribution and strain relaxation effect.

From this study, methods for analyzing the IQE of the GaN-based LEDs and its limiting factors are proposed and verified. It is also demonstrated that the p-type trench structure in the MQW will be the promising candidate for solving the efficiency droop problem of the GaN-based LEDs.

Key Words: GaN-based LEDs, internal quantum efficiency, efficiency droop, current-transient methodology, p-type trench structure

Student Number: 2008-20829

Contents

List of Tables

List of Figures

Chapter 1

Chapter 2

Chapter 3

Chapter 4

Chapter 1

Introduction

1.1 Background

During the last several years, GaN-based light emitting diodes (LEDs) (Fig. 1.1) have gradually substituted for conventional fluorescent lights in the fields of backlights of display and general lighting applications due to its advantages such as relatively long lifetime and high energy efficiency [1, 2]. Although the market size has increased and the efficiency of the GaN-based LEDs has improved rapidly [3-10], the general level of understanding of the physics remains insufficient [11, 12].

In order to reduce electric power consumption and increase light output power of the GaN-based LEDs, it is important to extract and analyze recombination coefficients and internal quantum efficiency (IQE) which is the relative probability of radiative recombination over the total recombination of injected carriers. There have been many

researches to analyze the IQE of the GaN-based LEDs and explain the origin of 'efficiency droop' (Fig. 1.2) which is the decrease of the IQE when current density increases [13-21]. However, there is no consensus on this problem yet [11, 12].

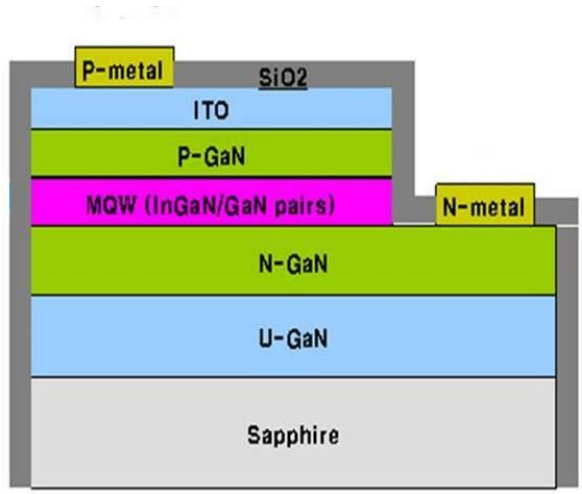

Fig. 1.1 Schematic cross-sectional view of the GaN-based LEDs.

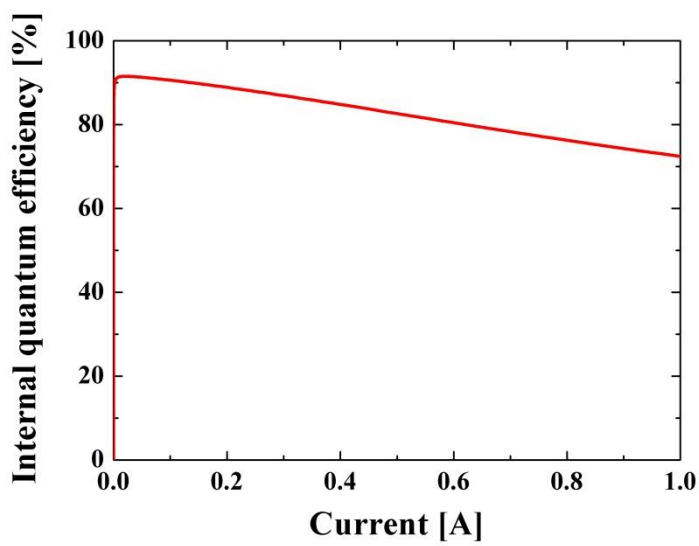

Fig. 1.2 Internal quantum efficiency of GaN-based LEDs showing efficiency droop at high current density.

The radiative recombination efficiency of GaN-based LEDs is very high (Fig. 1.3) despite the high trap density (Fig. 1.4) caused by the lattice mismatch with sapphire substrates [22]. Although there have been many studies to explain this phenomenon [23, 24], a generally accepted explanation has not yet been established. In addition, there have also been many studies to analyze the relationships between the traps and the 'efficiency droop' of GaN-based LEDs when high current flows. Some researchers concluded that trap density is not closely related to the efficiency droop [25]. In contrast, some other researchers explained that the traps are the main cause of efficiency droop [16, 26].

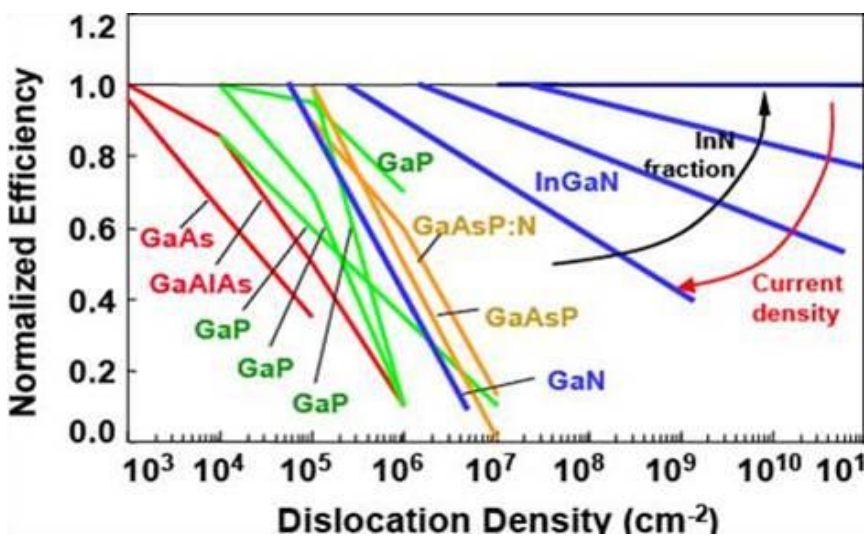

Fig. 1.3 Dependence of luminescence efficiency of various compound semiconductor materials on the dislocation density [22].

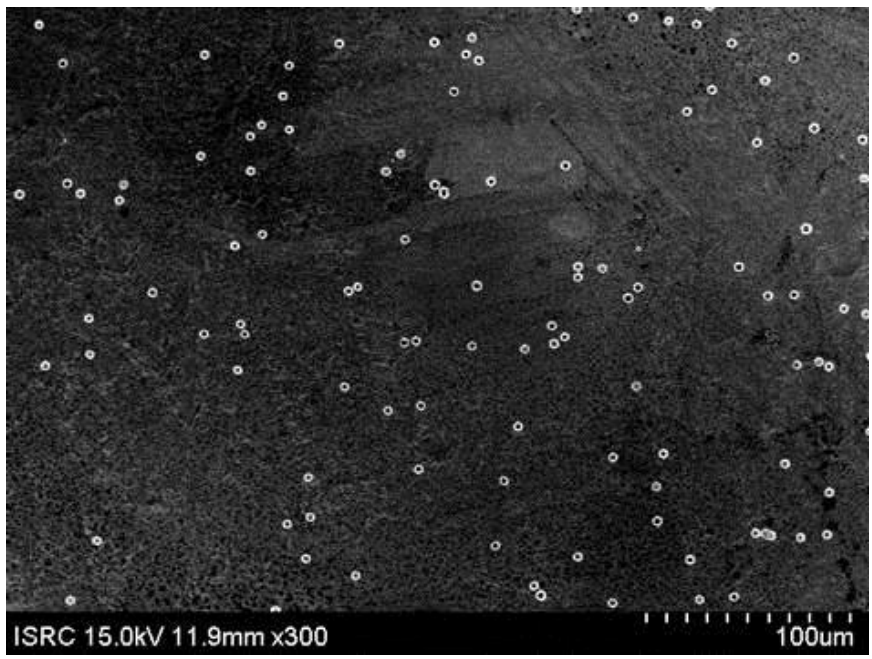

Fig. 1.4 Surface of GaN grown on a sapphire substrate showing high dislocation density.

1.2 Scope of thesis

In Chapter 2, the recombination coefficients and the IQE of the GaN-based LEDs are extracted by analyzing transient characteristics with the rate equation. In addition, the concept of the effective volume of the active region is proposed and applied to the to the rate equation of the LEDs

A temporal increase in the current of LEDs is found when a constant voltage is applied to the anode. The activation energy of the traps causing this abnormal behavior is extracted by current-transient methodology in Chapter 3. The process of current increase caused by the trapping was also analyzed by a TCAD simulation. In addition,

the effects of the traps on the electrical and optical characteristics of LEDs were predicted by a TCAD simulation and confirmed by measurement.

In Chapter 4, a novel structure using p-type trench in the MQW is proposed to solve the efficiency droop problem with an improvement of the poor hole transport characteristics and reduced quantum-confined stark effect (QCSE). In addition, the optical and electrical characteristics are compared with the conventional structure by using TCAD simulation and cathodo-luminescence (CL) measurement. Finally, in Chapter 5, the work will be concluded with summary and suggestions for future work.

Chapter 2

Extraction of IQE and recombination coefficients by measuring transient characteristics

2.1 Model description and experimental setup

The current continuity equation of carrier concentration injected into the active region can be written as Eq. (2.1a) while Eq. (2.1b) shows the solution of Eq. (2.1a). Since the initial carrier concentration (n_0) can be calculated from Eq. (2.2) and the optical power is proportional to $V_{active}Bn^2$, time-carrier concentration characteristics can be obtained by measuring the transient characteristics of the optical power. In addition, as Eq. (2.1b) shows the decaying characteristics of the carrier concentration (n), Shockley-Read-Hall (SRH) recombination coefficient (A), radiative recombination coefficient (B), and coefficient causing efficiency droop problem (C) of GaN-based LED can be extracted by fitting this equation to time-carrier concentration characteristics. In this equation, coefficient C includes Auger recombination coefficient

and leakage current caused by electron overflow which are proportional to n^3 [11].

$$-\frac{dn}{dt} = An + Bn^2 + Cn^3 \tag{2.1a}$$

$$t = \frac{1}{2A}\left[\frac{2B\tan^{-1}\left(\frac{B+2Cn}{\sqrt{4AC-B^2}}\right)}{\sqrt{4AC-B^2}} + \ln\left(A + n(B+Cn)\right) - 2\ln n\right] - t_0 \tag{2.1b}$$

$$t_0 = \frac{1}{2A}\left[\frac{2B\tan^{-1}\left(\frac{B+2Cn_0}{\sqrt{4AC-B^2}}\right)}{\sqrt{4AC-B^2}} + \ln\left(A + n_0(B+Cn_0)\right) - 2\ln n_0\right] \tag{2.1c}$$

(n_0 and t_0 represent initial carrier concentration and time, respectively*)*

$$I = qV_{active}(An + Bn^2 + Cn^3) \tag{2.2}$$

Figure 2.1 illustrates the experimental setup for the transient characteristics in optical power measurement. At first, a current pulse (100 mA (3.2 V) amplitude, 4 μs duration and 6 μs period) generated from 81110A pulse generator is applied to the prepared GaN-based LED sample. In order to reduce the change of the band structure and carrier sweep-out from the active region, the 'off' state bias is set to 2.4 V instead of 0 V. When the LED sample emits the optical signal caused by the current pulse, a fast response photo-receiver collects this optical signal and converts the optical signal to a voltage signal. This voltage signal is recorded by an oscilloscope. Since the transient characteristics can be obtained by applying a very short current pulse to the sample, recombination coefficients can be extracted rapidly by this method. And, as it is measured by applying operating current at room temperature, recombination

coefficients and the IQE are extracted under real operating circumstances.

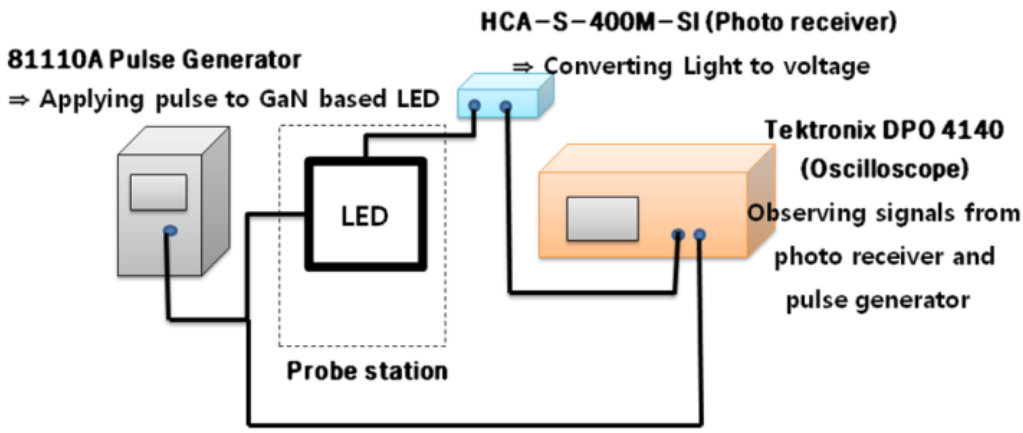

Fig. 2.1. Experimental setup for measuring transient characteristics of GaN-based LEDs.

2.2 Effective volume of the active region

For the calculation of the carrier concentration at each current from Eq. (2.2), the volume of the active region should be known. In order to increase radiative recombination of the electron-hole pairs, GaN-based LEDs employ multiple quantum well (MQW) structure [7]. However, the carrier concentration and recombination process of the GaN-based LEDs are not uniformly distributed in the MQW. Because of the polarization of nitride-based materials, the wave-function of electron and hole is not overlapped exactly in the quantum well [3]. Furthermore, as the effective mass of hole is much larger than that of electron [27] and the activation energy of Mg acceptor is high [28], most of the injected holes are concentrated in the single quantum well near

the p-GaN layer. Because of these characteristics of nitride-based materials, most of the recombination processes are concentrated in the small volume of the active region. As carrier concentration severely affects the IQE of the LEDs, carrier distribution in the active region should be considered when the volume of the active region is analyze and calculated [29].

The carrier distribution and the actual volume of active region are analyzed by TCAD simulation. In this simulation, the physical parameters of nitride-based materials are based on the research of I. Vurgaftman, et al [30]. Surface charges induced by spontaneous and piezoelectric polarizations are also considered [31]. Shockley-Read-Hall (SRH) recombination coefficient (*A*) and radiative recombination coefficient (*B*) are kept constant at 5.0×10^{6} s^{-1} and 1.0×10^{-11} $cm^{3}s^{-1}$, which are in the range of generally accepted values [12]. In the case of Auger recombination coefficient (C_{Auger}), theoretically calculated value (2.0×10^{-31} $cm^{6}s^{-1}$) is used [5]. If the overflow current needs to be considered, the value of *C* should be extracted experimentally. It is assumed, however, that the theoretical Auger recombination coefficient can be used as a first-order approximation in this calculation. The active region of the structure consists of five 3-nm-thick undoped $In_{0.2}Ga_{0.8}N$ QWs and four 6-nm-thick n-GaN (n-doping = $2 \times 10^{17}cm^{-3}$) barriers. The structure also includes 17.5-nm-thick p-$Al_{0.2}Ga_{0.8}N$ (p-doping = 5×10^{19} cm^{-3}) electron blocking layer (EBL) to avoid electron leakage from the MQW.

Figure 2.2(a) and (b) show the electron and hole concentration in the five quantum wells of the GaN-based LEDs calculated by TCAD simulation tools at current density of

10 mA and 1 A [32]. When the current is low (10 mA), both of electrons and holes are concentrated at the each side of the MQW. As current becomes higher (1 A), electrons spread in the MQW uniformly, but holes are still concentrated at the p-GaN side of the MQW because of heavy effective mass. Therefore, carriers are concentrated at the p-GaN side of the quantum well and recombination rate, especially Auger recombination ($C_n n^2 p + C_p n p^2$) caused by high hole concentration, increases rapidly in this small volume.

This 'effective volume' is defined and calculated as the Eq. (2.3) and (2.4).

$$\text{Volume correction factor} = \frac{\text{Total recombination in MQW}}{\text{Highest recombination rate} \times \text{Volume of the active region}} \quad (2.3)$$

$$\text{Effective volume } (V_{effective}) = \text{ Volume correction factor } \times \text{Physical volume } (V_{physical}) \quad (2.4)$$

The volume correction factor and the IQE of polar c-plane GaN-based LED having 5 MQW are calculated by a TCAD simulation. As shown in Fig. 2.3, effective volume is reduced as current is increased. Because of the reduced effective volume of active region, carrier concentration increases and IQE is reduced significantly as Auger recombination increases.

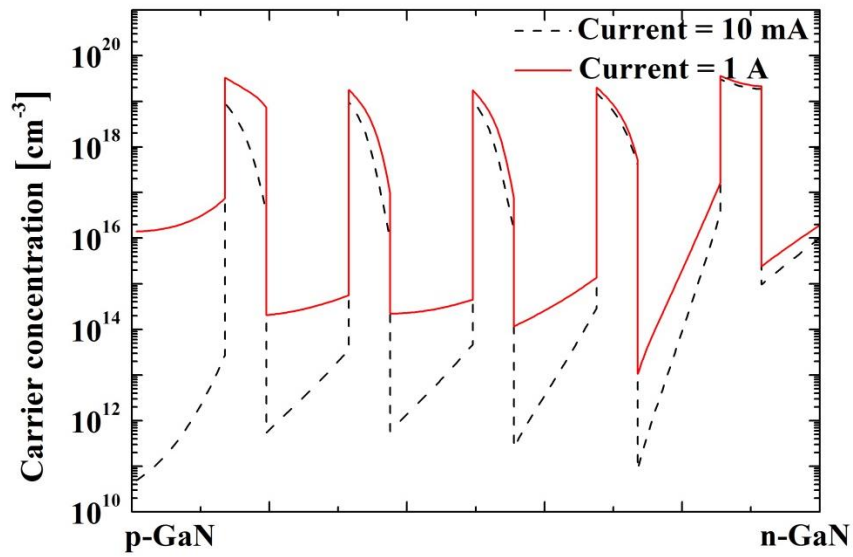

(a)

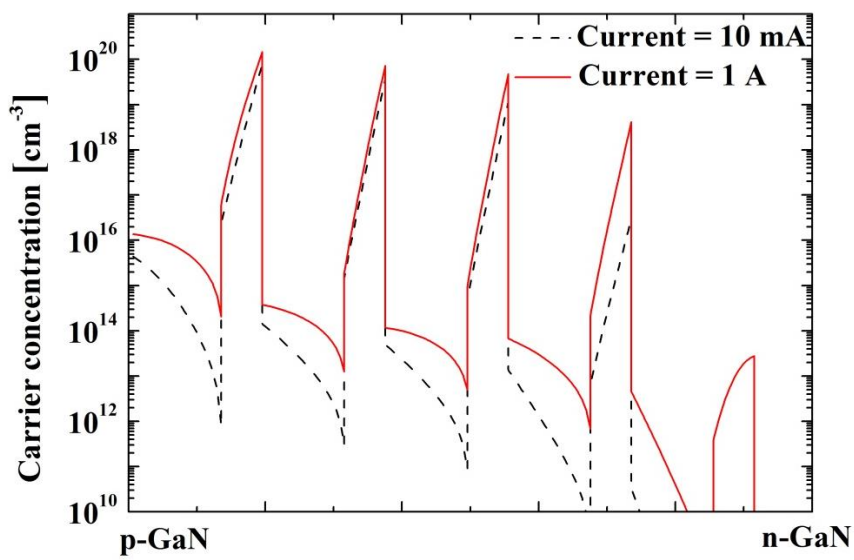

(b)

Fig. 2.2. Calculated (a) electron and (b) hole concentration in the MQW when 10 mA or 1 A current flows.

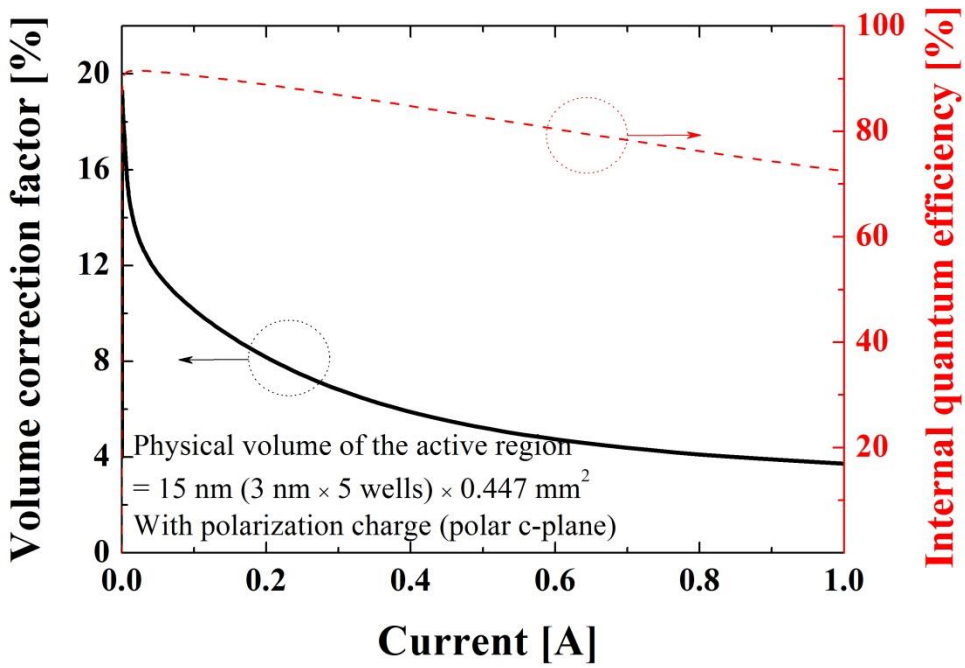

Fig. 2.3. Calculated volume correction factor and the IQE of polar c-plane GaN-based LED using 5 MQW structure.

For comparison, the volume correction factor and the IQE of non-polar (m-plane) MQW and SQW structure are also calculated and plotted in Fig. 2.4. Both structures have the identical physical volume of the active region with the polar (c-plane) MQW structure. In the case of non-polar MQW structure, since there is no polarization charge in the active region, the recombination process is distributed more uniformly in the single quantum well near the p-type GaN layer and the volume correction factor and the

IQE are improved as shown in Fig. 2.4(a) and (b). Figure 2.4(c) and (d) show the volume correction factor, the IQE and recombination rate of non-polar SQW structure. As the barriers between quantum wells blocking the transport of holes are removed, holes are injected more efficiently into the active region. As a consequence, the volume correction factor and the IQE of non-polar SQW structure are greatly improved even though the volume correction factor could not reach 100 % because of poor hole diffusion length. This result confirms that the IQE is influenced by the effective volume of the active region. In addition, the effective volume of the GaN-based LEDs can be changed by polarization charge, the barriers between quantum wells, and current density.

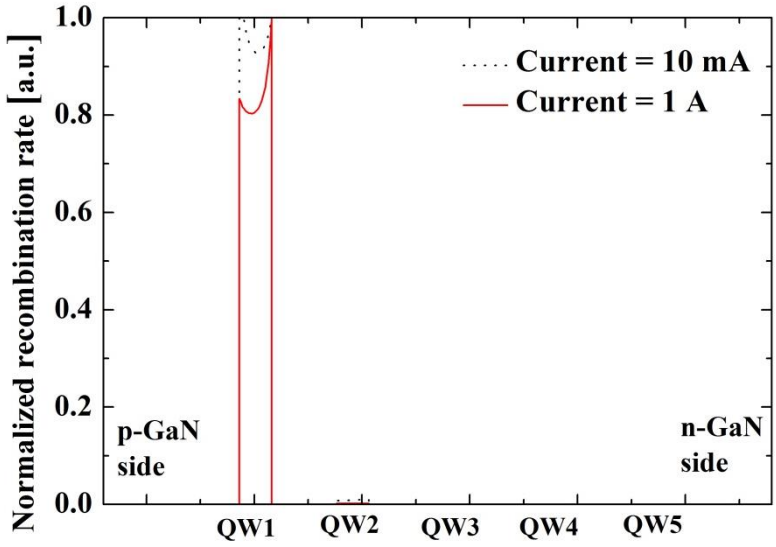
Normalized recombination rate [a.u.]
1.0
0.8
0.6
0.4
0.2
0.0
Current = 10 mA
Current = 1 A
p-GaN
side
n-GaN
side
QW1
QW2
QW3
QW4
QW5

(a)

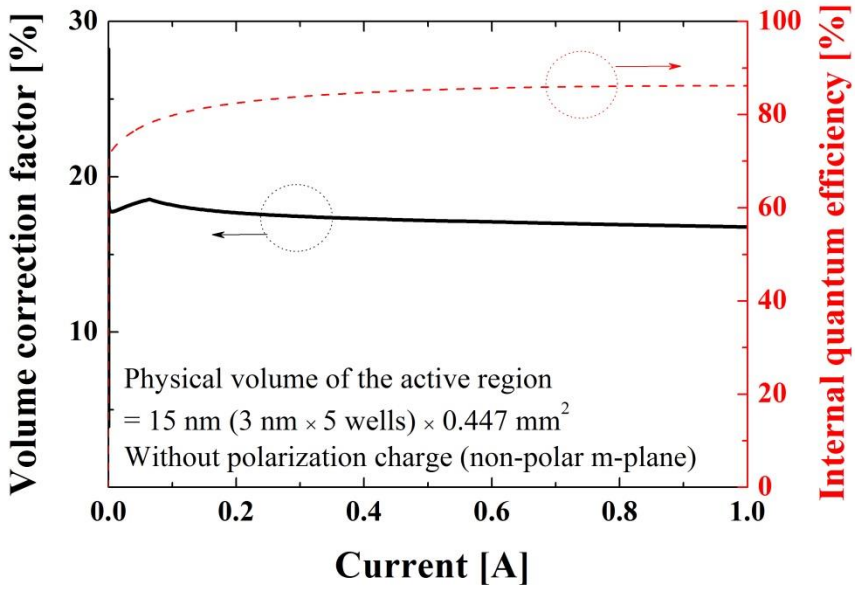
Volume correction factor [%]
30
20
10
Internal quantum efficiency [%]
100
80
60
40
20
0
Physical volume of the active region
= 15 nm (3 nm × 5 wells) × 0.447 mm²
Without polarization charge (non-polar m-plane)
0.0
0.2
0.4
0.6
0.8
1.0
Current [A]

(b)

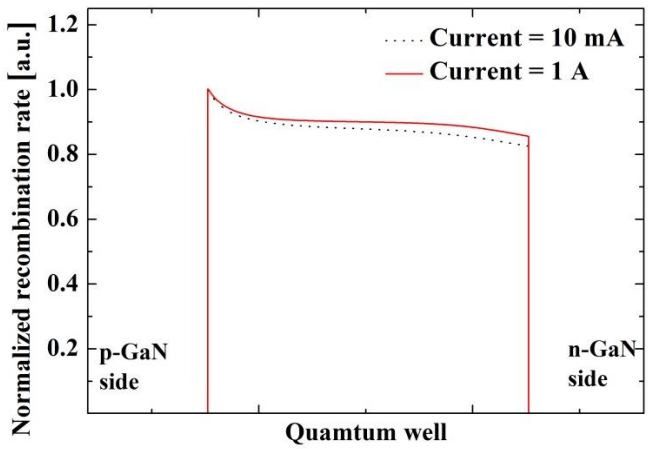

(c)

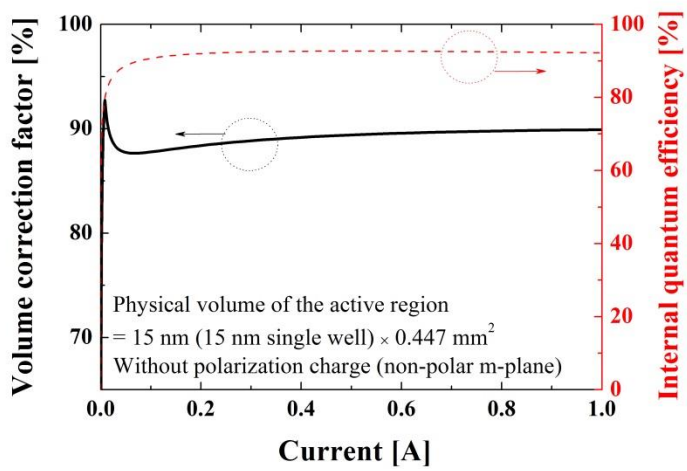

(d)

Fig. 2.4. Effects of the polarization field and barriers of the MQW on the volume correction factor and the IQE. In order to confirm the effect of the polarization field, the calculated effective volume and the IQE of non-polar m-plane GaN-based LED using five MQW structure are analyzed (a), and the distribution of the recombination rate in the MQW is shown (b). To analyze the effect of the barriers, the same simulations are conducted for non-polar m-plane GaN-based LED using single quantum well structure (c), (d).

2.3 Extraction of recombination coefficients

Transient characteristics of the light output power obtained by this experiment are illustrated in Fig. 2.5(a). As already mentioned, carrier concentration vs. time characteristics can be obtained by measuring the light output power as a function of time. Figure 2.5(b) shows the carrier concentration vs. time characteristics of an LED sample for two cases: (1) the physical volume or (2) the effective volume is used as the volume of the active region. By fitting the transient characteristics of carrier concentration to Eq. (2.1b), recombination coefficients are extracted as can be seen in Table 2.1. When the physical volume is used for calculating carrier concentration, the extracted Auger recombination coefficient is $5.1(\pm 0.2) \times 10^{-30}$ cm^6 s^{-1}, much higher than the theoretically calculated Auger recombination coefficient [5]. In contrast, when the effective volume is applied, the calculated carrier concentration becomes much larger, and the extracted Auger recombination coefficient is $1.9(\pm 0.2) \times 10^{-31}$ cm^6 s^{-1} which is similar to the theoretically calculated value. In addition, the extracted SRH and radiative recombination coefficients are also in the range of generally accepted values [12]. This result shows that the proposed model considering the effective volume of the active region is reasonable and more accurate than the conventional model using the physical volume.

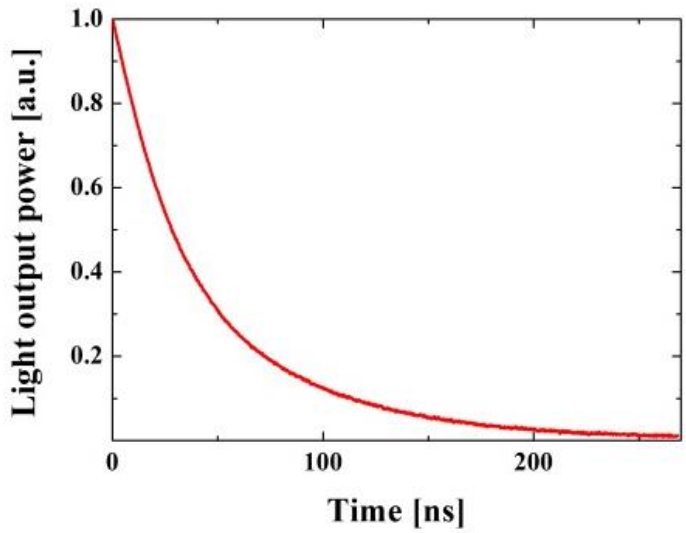

(a)

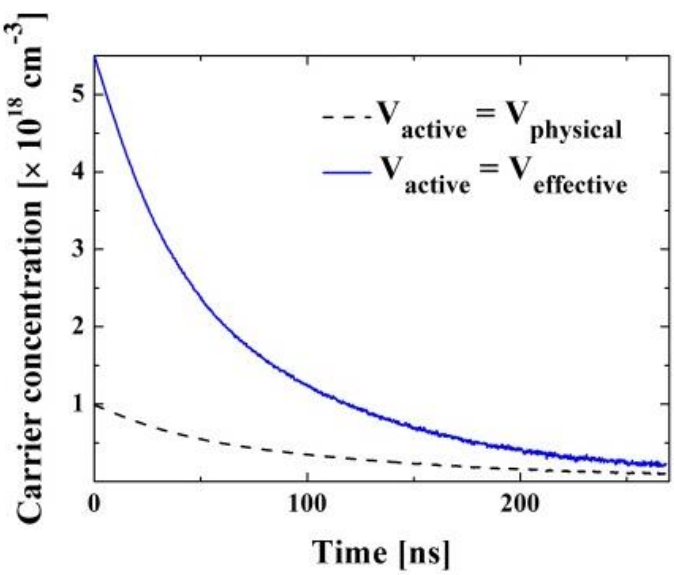

(b)

Fig. 2.5. Measured transient characteristics of the light output power (a) and the calculated carrier concentration (b) after the current pulse is applied to the LED sample. When the effective volume is used, the calculated carrier concentration becomes much larger.

Table 2.1. Calculated recombination coefficients by measuring transient characteristics

V_{active}	A (s^{-1})	B ($cm^3 s^{-1}$)	C ($cm^6 s^{-1}$)
$V_{physical}$	$5.2(\pm0.1) \times 10^{6}$	$3.0(\pm0.3) \times 10^{-11}$	**$5.1(\pm0.2) \times 10^{-30}$**
$V_{effective}$	$8.4(\pm0.1) \times 10^{6}$	$1.3(\pm0.3) \times 10^{-11}$	**$1.9(\pm0.2) \times 10^{-31}$**

2.4 Calculation of internal quantum efficiency

Figure 2.6 shows the calculated IQE using the physical volume or the effective volume of the active region and the IQE measured by light output power measurement with correctly calibrated light extraction efficiency. Recombination coefficients extracted by transient measurements (Table 2.1) are used to calculate the IQE. The calculated IQE based on the physical volume shows significant difference from the result of the light output power measurement. In contrast, the calculated IQE based on the effective volume shows good agreement with the result of the light output power measurement. Figure 2.7(a) and (b) show the measured transient characteristics and the calculated IQE of GaN-based LEDs having different size of active area. As the carrier concentration of the smaller LED is higher than that of the larger LED, carrier recombination happens faster as shown in Fig. 2.7(a). In addition, the ‘efficiency droop’ problem of the smaller LED is more serious because of the high carrier concentration as shown in Fig. 2.7(b).

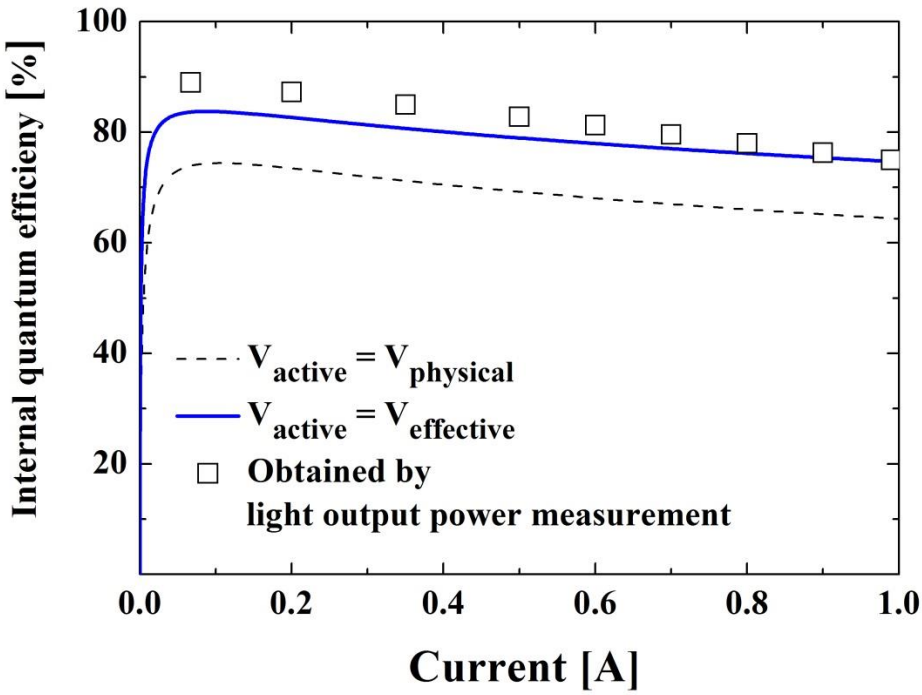

Fig. 2.6. Calculated IQE applying the physical volume or the effective volume of the active region and the IQE obtained by light output power measurement.

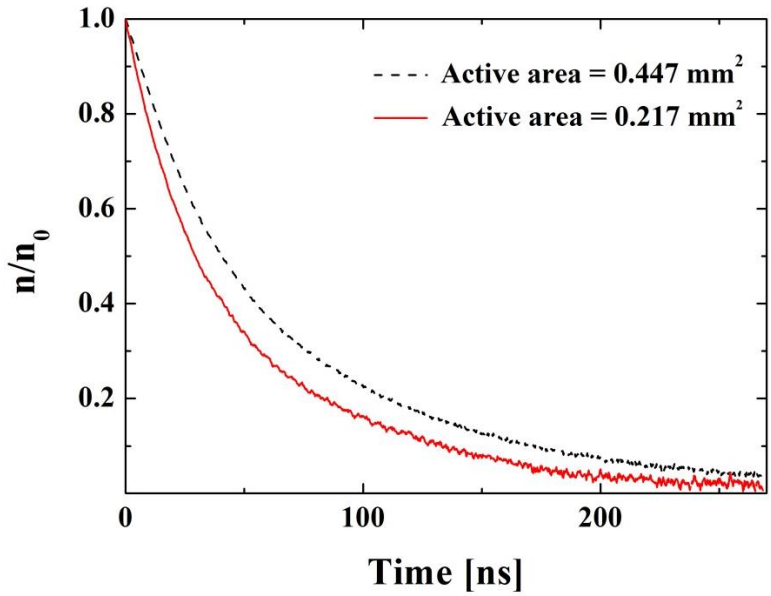

(a)

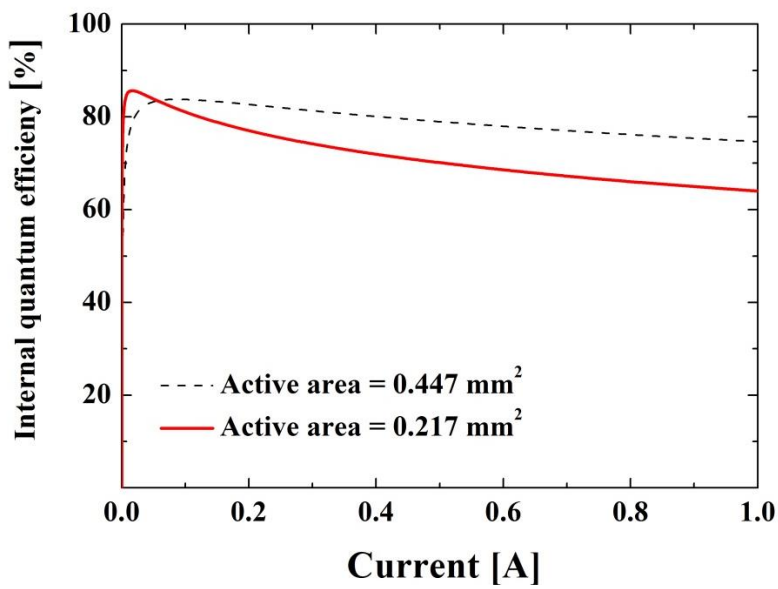

(b)

Fig. 2.7. (a) Measured transient characteristics and (b) calculated IQE of GaN-based LEDs having different size of active area.

The proposed model considering the effective volume of the active region can also explain the symmetry issue of the IQE and the origin of the efficiency droop. Figure 2.8 shows the IQE as a function of the square root of light output power, which is plotted in logarithmic scale. When the conventional rate equation is used for calculating the IQE of the LEDs, the square root of light output power is proportional to the carrier concentration (n) and the IQE should show symmetry about the peak IQE line. However, the experimental IQE shows significant asymmetry, unlike the result that the conventional equation predicts [33]. This symmetry problem of the IQE can be explained by considering the effective volume when the carrier concentration increases. As we already confirmed in Fig. 2.3, the effective volume is not constant and decreases as the carrier concentration increases. Therefore, as the light output power increases, injected carriers are more crowded in a small volume and the carrier concentration becomes higher than that predicted by the conventional rate equation. This higher carrier concentration in the effective volume is the origin of the asymmetry of the IQE and the severe efficiency droop.

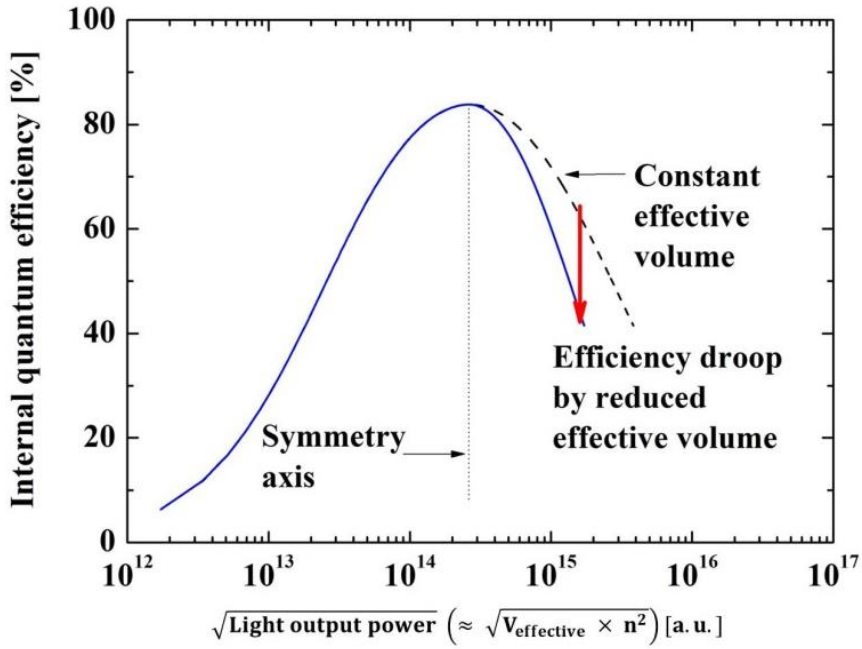

Fig. 2.8. Calculated IQE applying the effective volume of the active region as a function of the square root of light output power.

Chapter 3

Analysis of trap and its impact

3.1 Experimental procedure

In this chapter, a temporal increase in the current of LEDs is analyzed when a constant voltage is applied to the anode. The activation energy of the traps causing this abnormal behavior is extracted by current-transient methodology and CL measurement. The process of current increase caused by the trapping was also analyzed by a TCAD simulation. In addition, the effects of the traps on the electrical and optical characteristics of LEDs were analyzed by a TCAD simulation and measurement.

The electrical properties of the LED samples were analyzed using Agilent 4156C, and the light output power generated from the LEDs was collected by an optical fiber and measured by a photodiode (Femto HCA-S-400M-SI-FS). Gatan mono CL4 was used for CL measurement.

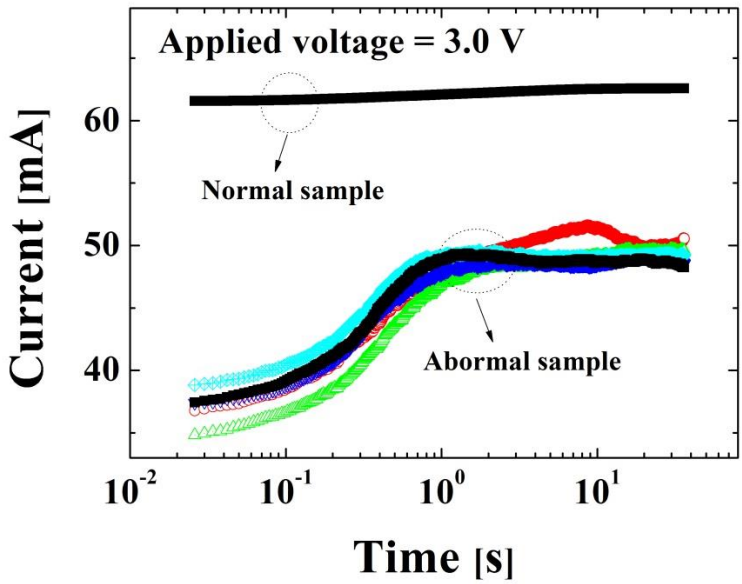

(a)

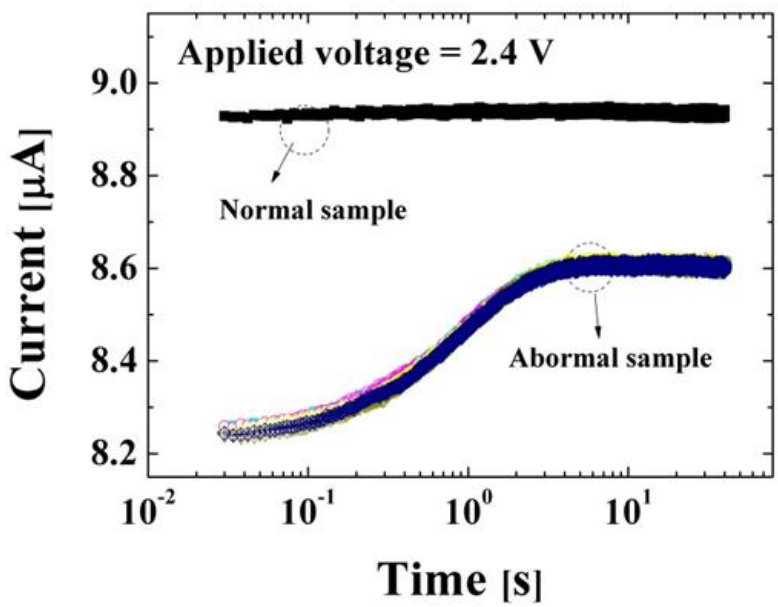

(b)

Fig. 3.1. Current-transient characteristics when a constant voltage ((a) 3.0 V and (b) 2.4 V) is applied. The same measurements are repeated five times without an interval.

3.2 Extraction of trap activation energy

In order to check the electrical characteristics of the LED samples, current was measured every 4 ms when a constant voltage is applied. Some of the as-prepared LED samples show abnormal electrical characteristics as shown in Fig. 3.1. When a constant voltage is applied to the anode, most of samples show constant current. However, the current of some samples increases slowly and becomes saturated after 3-5 s. When a high voltage (3.0 V) is applied and a high current flows, as shown in Fig. 3.1(a), the junction temperature increases and influences the current. Therefore, it is difficult to obtain repeatable current-transient characteristics. In order to eliminate the influence of junction temperature and guarantee the repeatability of the experiments, a much lower voltage (2.4 V) is applied and the current measurements are repeated five times without an interval. As shown in Fig. 3.1(b), the measurement results are nearly identical. To find the origin of the abnormality, the time interval between repeated measurements is changed and the results are compared. The measurement results in Fig. 3.2 show that the current increase due to the measurement completely reverses during a five-minute interval. Given this result, it can be assumed that this abnormal process is reversible similarly to the trapping and de-trapping process. In addition, the reversed current characteristics also show that the abnormal process is related to the trapping process. Figure 3.3(a) and 3.3(b) show the current-transient and the reverse current characteristics of the three abnormal samples. As shown in these figures, the sample showing a higher leakage current also shows a greater increase in current when a

constant voltage is applied. As it is known that a higher reverse leakage current flows with the increase in the amount of traps [34], it is expected that the abnormal increase in current would become severe when the trap density increases.

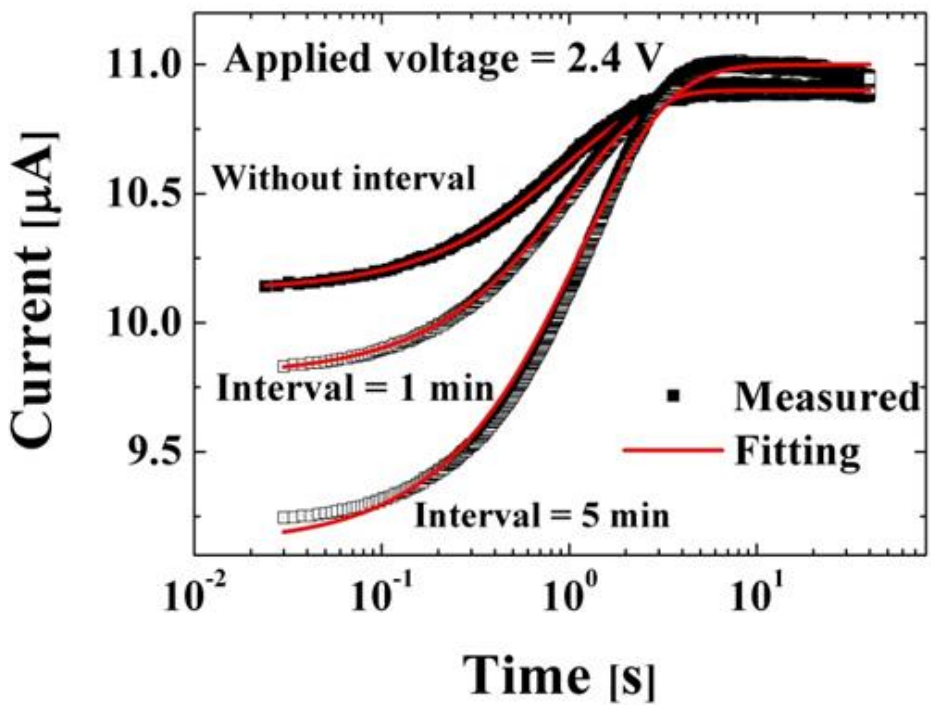

Fig. 3.2. Current-transient characteristics measured at different measurement intervals.

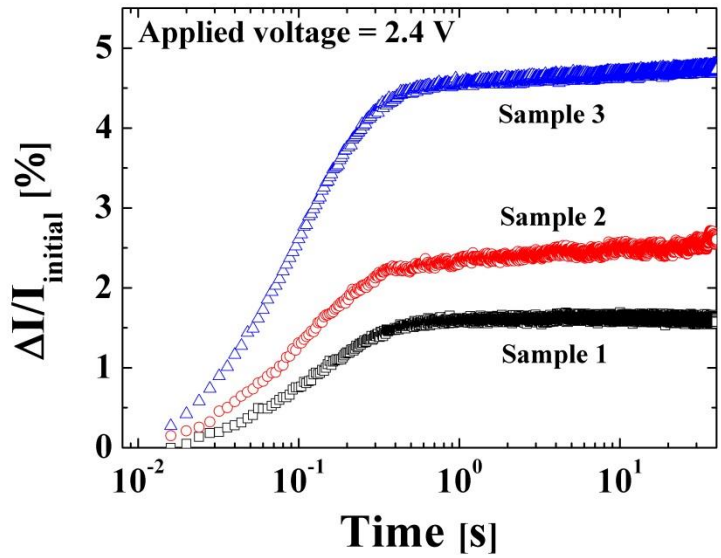

(a)

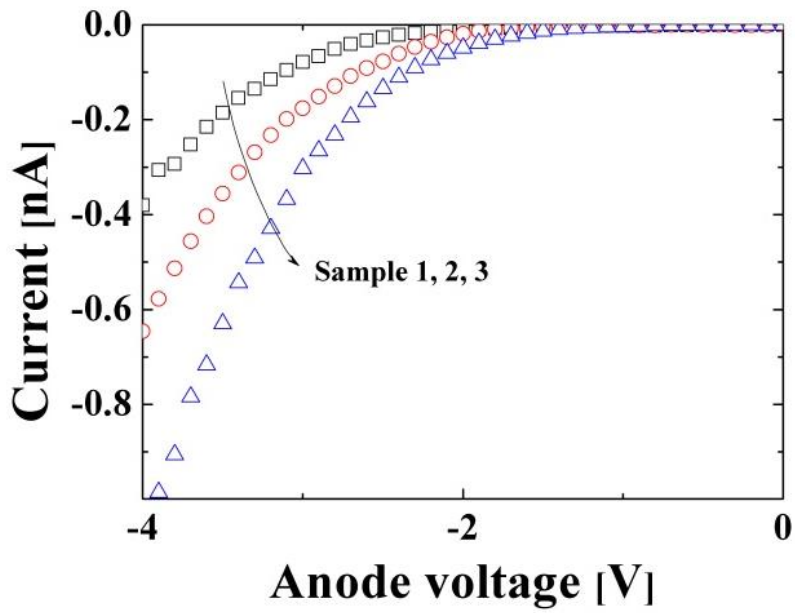

(b)

Fig. 3.3. (a) Current-transient characteristics and (b) reverse current characteristics of three abnormal samples.

On the basis of the assumption that the abnormality originates from the trapping process, we analyzed the current-transient characteristics by fitting them using Eq. (3.1), which models the increased current as the sum of pure single exponential terms [35, 36].

$$I_{fitted} = \sum_{i=1}^{n} \alpha_i \exp(-\frac{t}{\tau_i}) + I_{\infty} . \qquad (3.1)$$

Each single exponential term means the change in the current influenced by the traps having the time constant τ_i. I_{∞} in this equation means the saturated current when time goes to infinity. In this research, a total of 50 single exponential terms with time constant, which are equally spaced logarithmically in time, are used for fitting the experimental result. The fitting is performed to minimize the sum of $|I_{measured} - I_{fitted}|^2$ by controlling the α_i's of each single exponential term. In this way, we can determine the time constant of the traps affecting the current increase by comparing the obtained α_i's. The current-transient characteristics shown in Fig. 3.2 are fitted using Eq. (3.1). Figure 3.4 shows the time constant (τ_i) of traps and the change in its amplitude as the interval becomes longer.

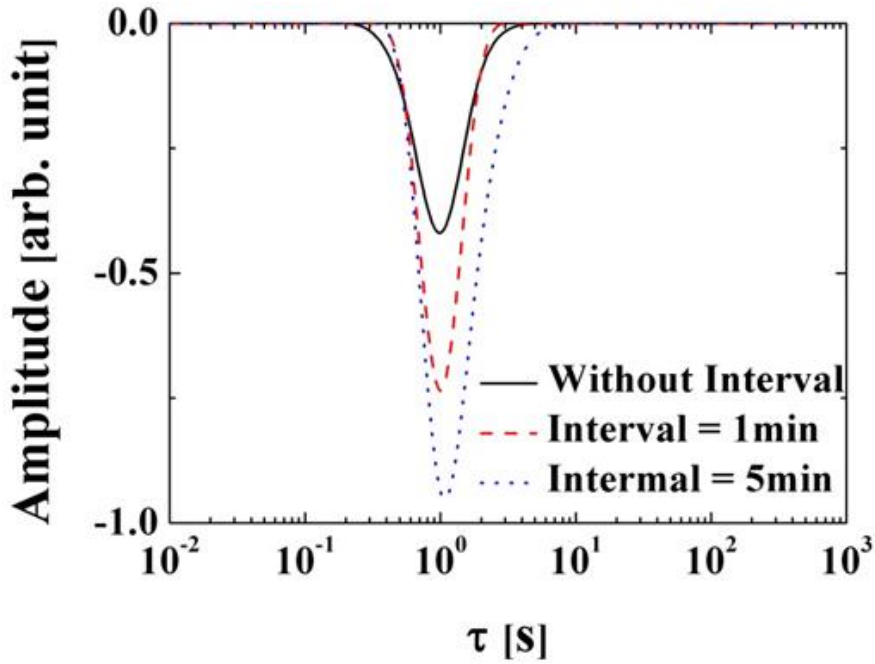

Fig. 3.4. Time constant spectrum with measured at different intervals. Amplitudes of all time constants are obtained by the fitting process.

From this result, we can extract a time constant of trapping of 1 s, which causes the increase in current. In order to calculate the activation energy of the trap, the current-transient characteristics are measured under different temperature conditions (Fig. 3.5(a)). These time constants at different temperatures are plotted as an Arrhenius plot, and the estimated activation energy of the traps is 0.30 eV (Fig. 3.5(b)).

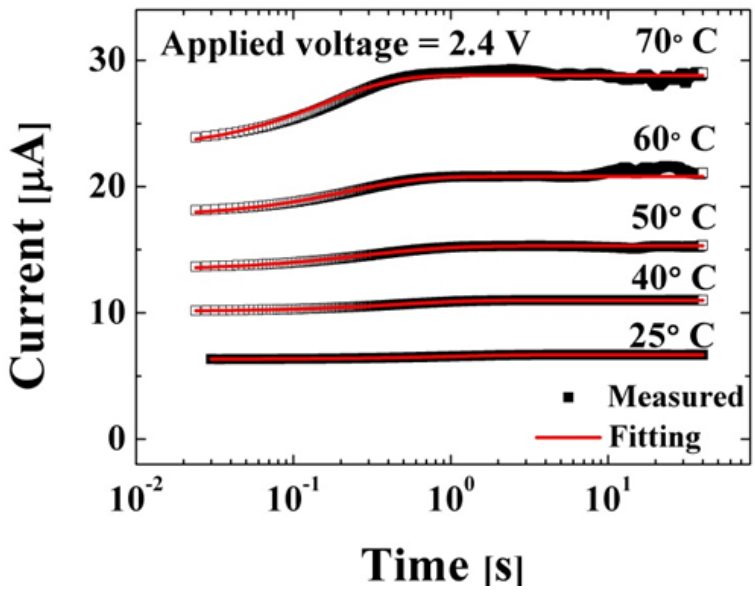

(a)

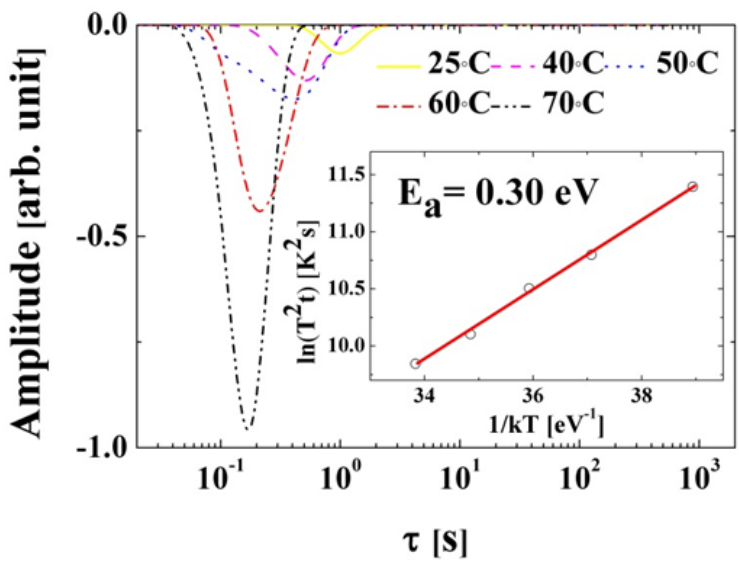

(b)

Fig. 3.5. (a) Current-transient characteristics under different temperature conditions. (b) Time constant of different measurement temperatures and the extracted activation energy of the trap (inset).

This result is consistent with the CL spectra of LED samples.30) CL spectra can be constructed by plotting the light output power generated by injected electrons as a function of wavelength. In this experiment, CL image and spectra are analyzed at room temperature to obtain the activation energy of traps. Figure 3.7(a) and 3.7(b) show the CL spectra of the LED sample surface shown in Fig. 3.6. The CL spectrum shows a luminescence peak of 2.3-2.4 eV, which is 0.3-0.4 eV smaller than the bandgap of the MQW and consistent with the trap activation energy calculated by current-transient methodology.

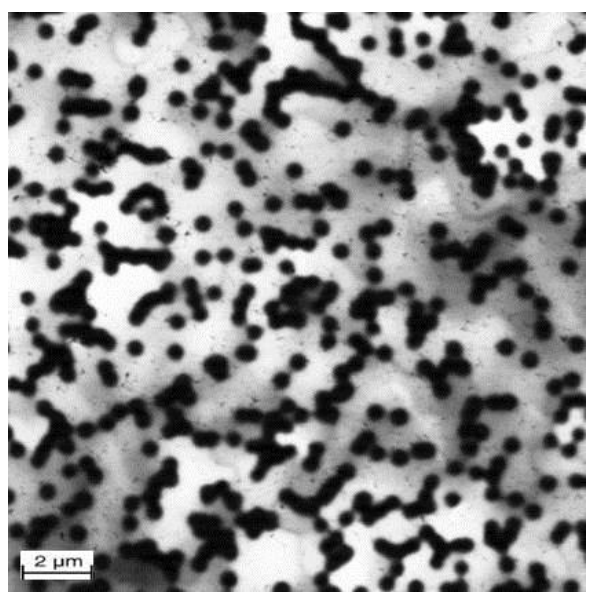

Fig. 3.6. Cathodo-luminescence (CL) image of GaN-based LED.

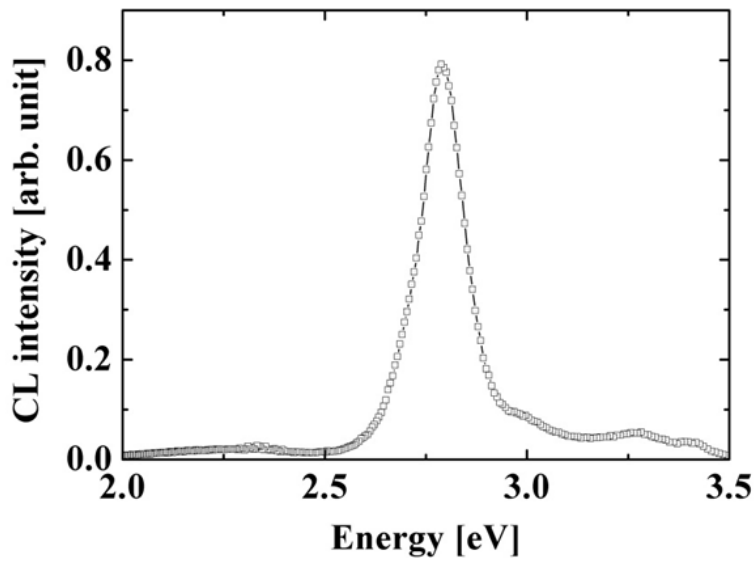

(a)

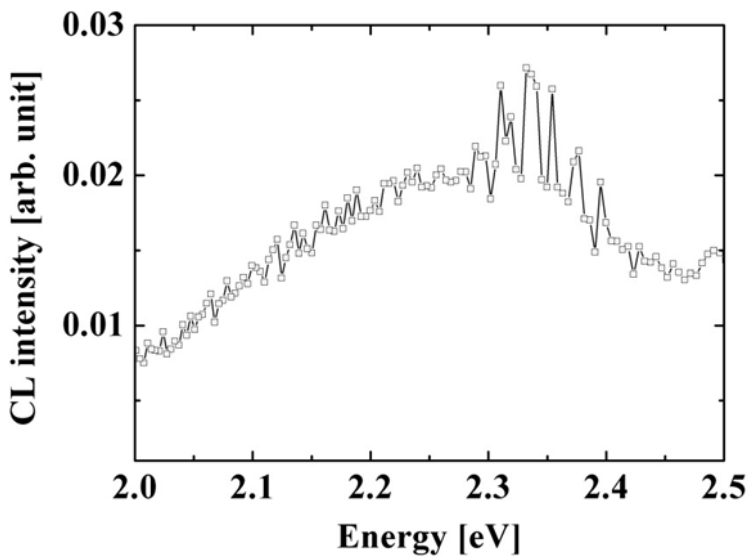

(b)

Fig. 3.7. CL spectrum showing (a) a main peak of 2.7 eV and (b) a peak of 2.3 ~ 2.4 eV peak originating from the trap.

3.3 Effects of traps on GaN-based LEDs

To find the relationship between the trapping process and the increase in current, a simulation of GaN-based LEDs is conducted [32]. The physical parameters of nitride-based materials are based on the research of I. Vurgaftman, et al [30]. As the LED samples are grown on c-plane sapphire substrates, we also considered the polarization field induced by the difference in lattice constant [31]. The negatively charged trap situated at 0.3 eV above the valence band of GaN is probably a Ga vacancy, which is considered as the origin of the yellow luminescence [37]. In this simulation, the capture cross section of the trap is 10^{-16} cm^{-2}, which is in the range of generally accepted values [37]. Trapped hole concentration and conduction band are shown in Fig. 3.7(a). Figure 3.7(b) shows increase in current obtained by TCAD simulation. The barrier height of the MQW is reduced by the hole trapping process and the current is increased by this barrier lowering. As can be seen in Figs. 3.3(a) and 3.11, the increase in the current ($\Delta I/I_{initial}$) of the abnormal samples is distributed between 1 and 5% of the initial current. From the simulation results shown in Fig. 3.9, it is confirmed that current increases by 1.8 and 9.8% of the initial current when the trap densities are 10^{17} and 10^{18} cm^{-3}, respectively. Therefore, it can be assumed that the trap density of the measured LED samples is distributed in this range.

As shown in Figs. 3.8 and 3.9, it is confirmed that the trapped charge changes the height of the barriers and the electrical characteristics of the LEDs. Trap density also has a strong influence on the optical characteristics of the LEDs as well as the electrical

characteristics [38]. The internal quantum efficiency of the LEDs can be represented by Eq. (3.2), where *n*, *A*, *B*, and *C* represent the carrier concentration in the active region, SRH recombination coefficient determined by trap density, radiative coefficient, and coefficient causing efficiency droop problem, respectively:

$$IQE = \frac{Bn^2}{An+Bn^2+Cn^3} \tag{3.2}$$

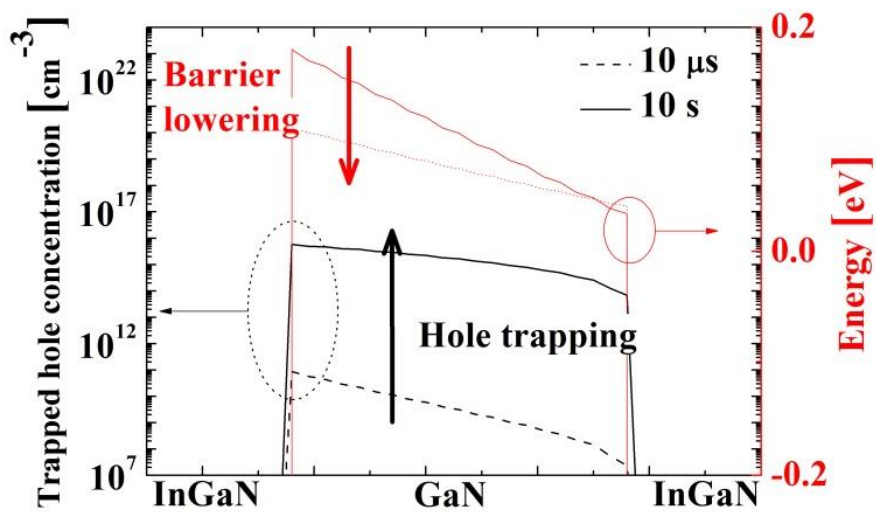

Fig. 3.8. Trapped hole concentration and conduction of the MQW when 2.4 V is applied to the anode (trap density = 10^{16} cm^{-3}).

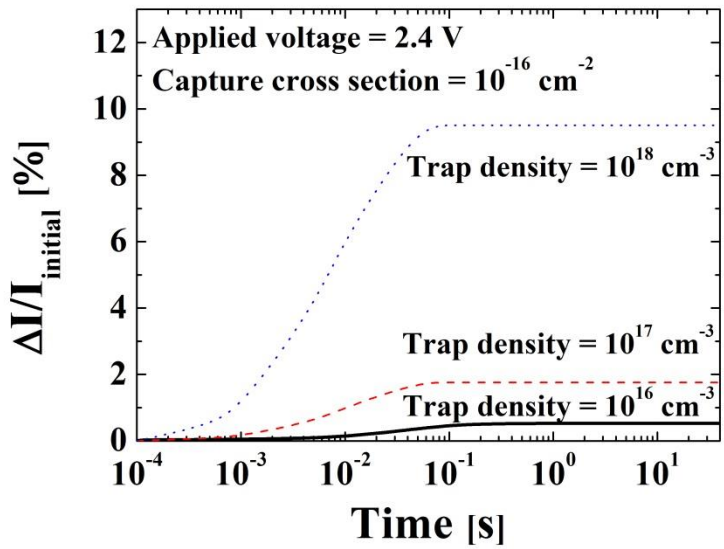

Fig. 3.9. Current-transient characteristics obtained by TCAD simulation.

In order to confirm the effect of traps, the recombination rate in the MQW and the internal quantum efficiency are confirmed by TCAD simulation when the trap density is changed. In this simulation, the radiative recombination B and the Auger recombination coefficient, C_{Auger} are kept constant at 1.0×10^{-11} cm^3s^{-1} and 2.0×10^{-31} cm^6s^{-1}, which are in the range of generally accepted values. Figures 3.10(a) and (b) show the calculated SRH recombination rates in the MQW and the internal quantum efficiency of the LEDs. From the results, it is found that the SRH recombination rate increases and the internal quantum efficiency is reduced as trap density increases. The measurement result in Fig. 3.11 also shows that the LED samples with a larger abnormal current increase show a reduced light output power.

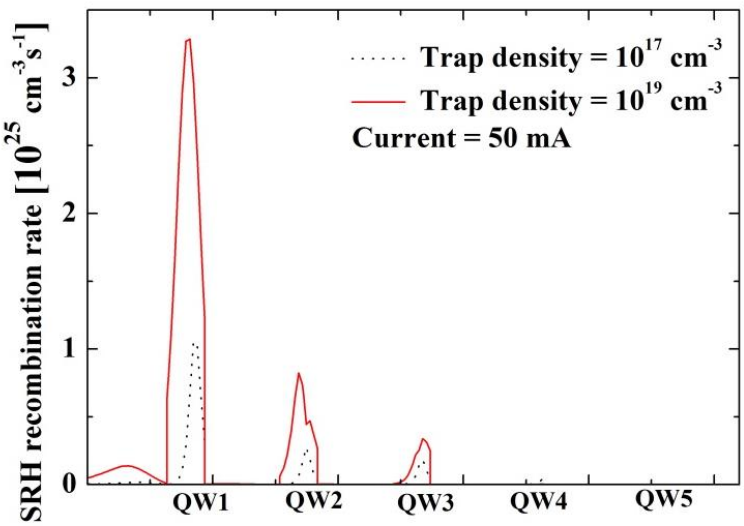

(a)

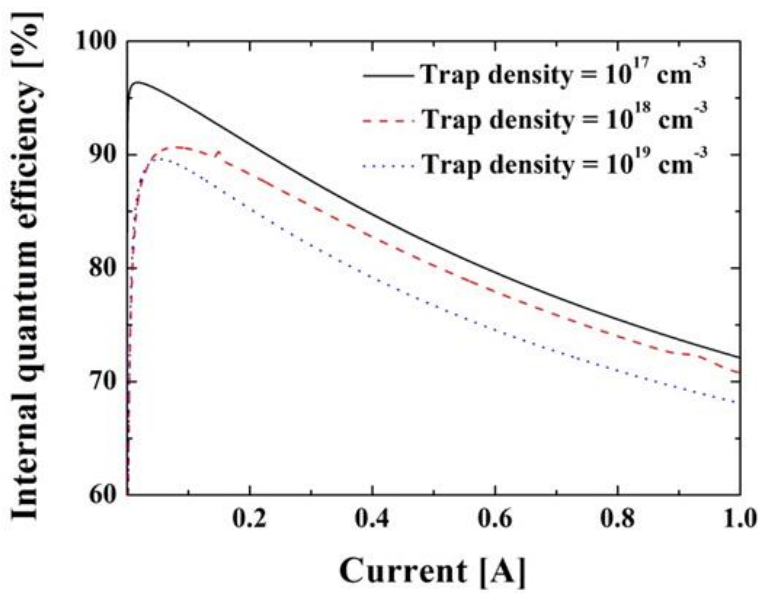

(b)

Fig. 3.10. (a) SRH recombination rates in the MQW obtained by TCAD simulation. (b) Internal quantum efficiency of the LEDs obtained by TCAD simulation.

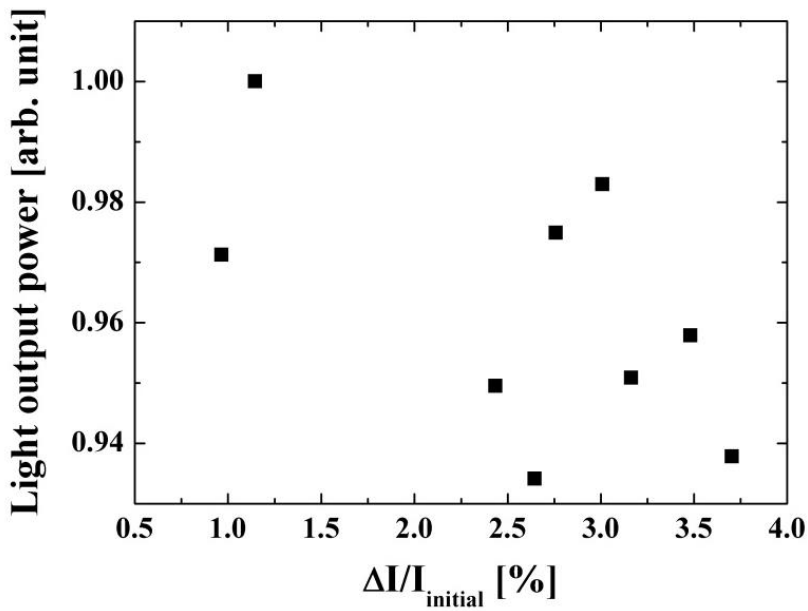

Fig. 3.11. Measured light output power of the abnormal samples when 100 mA current flows.

The effect of traps on the reliability characteristics is also analyzed. Figure 3.12(a) shows the current-transient characteristics of an abnormal sample (Sample A) and a normal sample (Sample B). Time-dependent light output power of Sample A and Sample B is measured at high temperature (120°C) when 100 mA current flows. The measurement result in Fig. 3.12(b) shows that light output power of Sample A degrades faster than that of the Sample B due to the high trap density in the MQW layer.

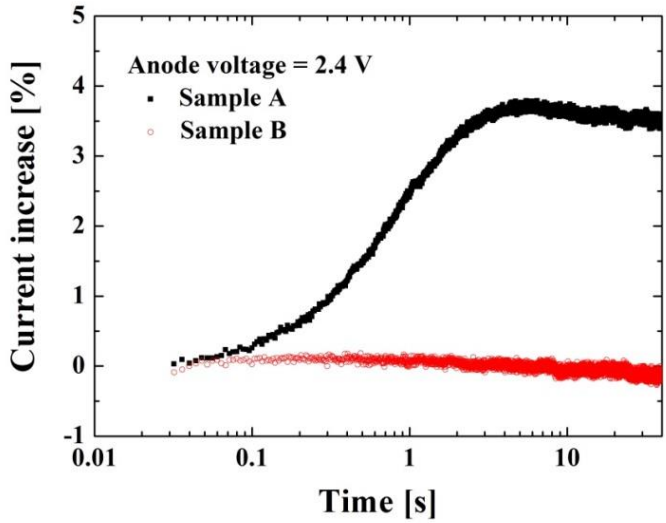

(a)

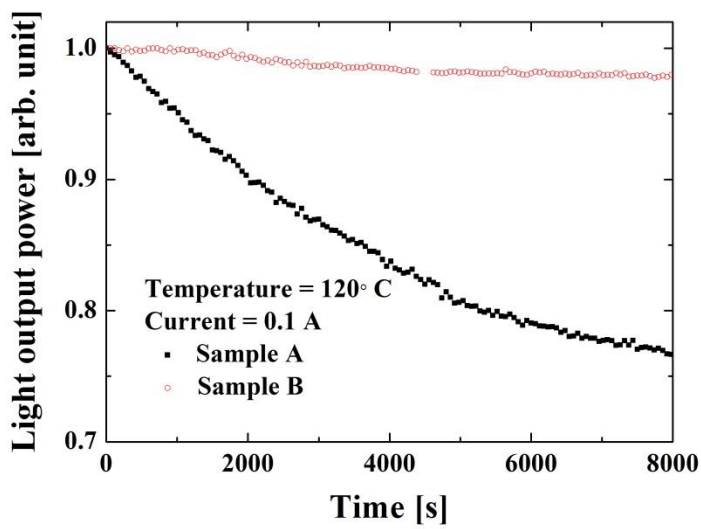

(b)

Fig. 3.12. (a) Current-transient characteristics of an abnormal sample (Sample A) and a normal sample (Sample B). (b) Time-dependent light output power of Sample A and Sample B measured at high temperature (120°C) when 100 mA current flows.

Chapter 4

p-type trench structure for improving IQE

4.1 Proposed structure

Although there is still no clear consensus on the origin of the ‘efficiency droop’ problem [11, 12], it is generally accepted that insufficient hole transport characteristics of nitride-based material is strongly linked with the efficiency droop problem [29]. Although Multi-Quantum Well (MQW) layers are used in the LEDs, most light of GaN-based LEDs is emitted in the single quantum well nearest to the p-GaN side because of the poor hole transport characteristics [39]. This localized emission increases Auger recombination rate and makes severe efficiency droop at high current density.

In this chapter, a novel structure using p-type trench in the MQW is proposed to solve this problem and improve the poor hole transport characteristics. Figure 4.1 shows

a bird's-eye view of the proposed structure. p-type trenches are extended from the electron blocking layer and inserted periodically into the MQW layer. Figure 4.2 shows the expected advantage of these p-type trenches. Hole transport of nitride-based material is insufficient because of high activation energy of Mg acceptors [28] and its heavy effective mass [27]. This limits electron-hole pair recombination of nitride based LEDs into the single well near the p-GaN, although the MQW layers are used for increasing recombination layer as shown in Fig. 4.2(a). In contrast, p-type trench effectively spreads the holes into the MQW and internal quantum efficiency (IQE) is improved (Fig. 4.2(b)).

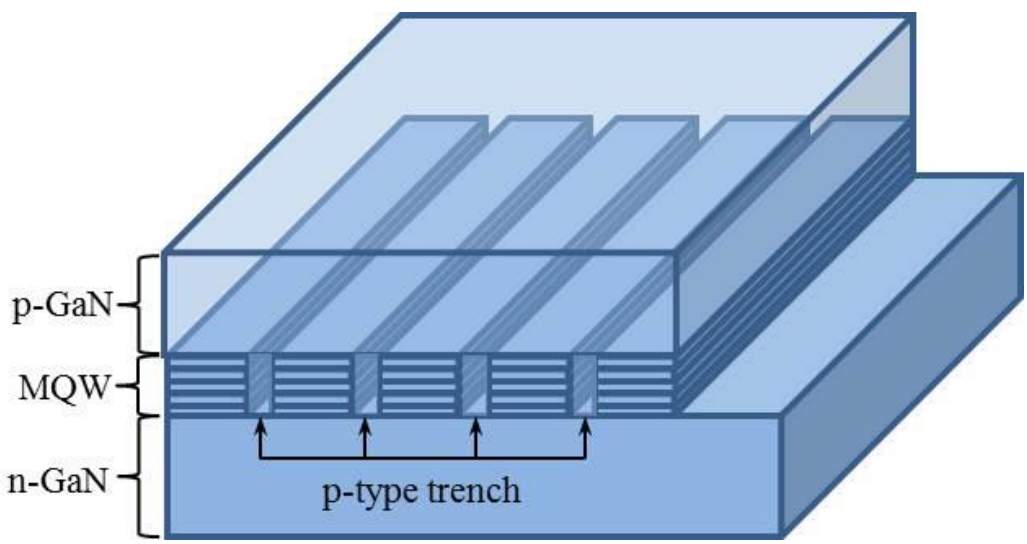

Fig. 4.1. A bird's-eye view of the p-type trench LED for improving IQE.

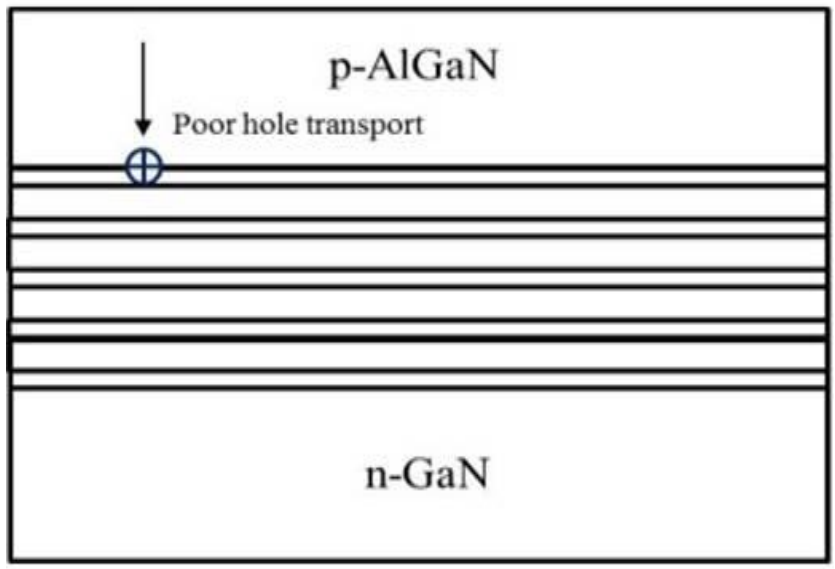

(a)

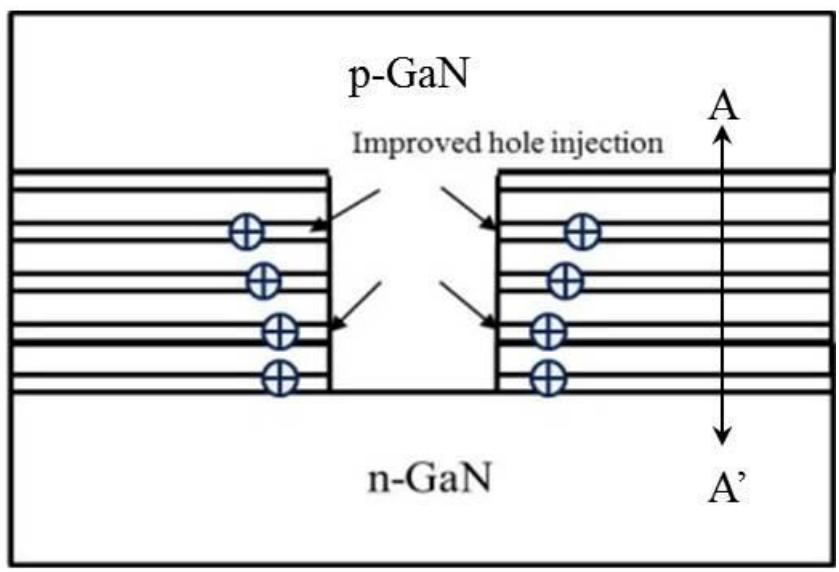

(b)

Fig. 4.2. Hole distribution in the MQW of (a) the conventional LED and (b) the p-type trench LED.

The optical and electrical characteristics of the conventional structure (without trench) and the proposed structure (with p-type trench) are analyzed by using Silvaco simulation tools. The MQW layer consists of five 3-nm-thick $In_{0.2}Ga_{0.8}N$ QWs, separated by four 6-nm-thick GaN barriers. Physical parameters of nitride-based materials are based on the research of I. Vurgaftman, et al [30]. Band offset ratio ΔE_c : ΔE_v at InGaN/GaN interfaces and AlGaN/GaN interfaces is assumed to be 55 : 45. Polarization charges induced by spontaneous and piezoelectric field are also considered. As it is known that this built-in polarization charges are partially compensated by fixed defects and interface charges [40], 73 % of the theoretical value is applied for this TCAD simulation. For an accurate calculation of carrier transport characteristics, transport model in the simulation includes thermionic emission and tunneling current in heterojunctions as well as drift-diffusion current [41]. Shockley-Read-Hall (SRH) recombination coefficient (*A*) and radiative recombination coefficient (*B*) are kept constant at 5.0×10^{6} s^{-1} and 1.0×10^{-11} cm^3s^{-1}, which are in the range of generally accepted values. In the case of Auger recombination coefficient (C_{Auger}), theoretically calculated value (2.0×10^{-31} cm^6s^{-1}) is used.

4.2 Simulation results

Figure 4.3 shows the calculated hole concentration for the conventional LED and the p-type trench LED cut through the A-A' line of Fig. 4.2. Figure 4.4(a) and (b) show

the calculated radiative recombination rate for the conventional LED and the p-type trench LED, respectively. And Figure 4.4(c) shows the calculated radiative recombination rate cut through the A-A' line of Fig. 4.2.The width of the p-type trench and the distance between the trenches are 50 nm and 1 μm, respectively. In the case of the conventional structure, holes are concentrated at the single quantum well near the p-GaN layer and the recombination rate is also crowded in the single quantum well because of large hole effective mass. In contrast, holes are effectively injected and spread into the quantum wells near the n-GaN side and radiative recombination rates are improved by using the p-type trench in the MQW. The IQE characteristics are also confirmed by the TCAD simulation as shown in Fig. 4.5. Efficiency droop is reduced and IQE of p-type trench is 12 % higher at 1A current.

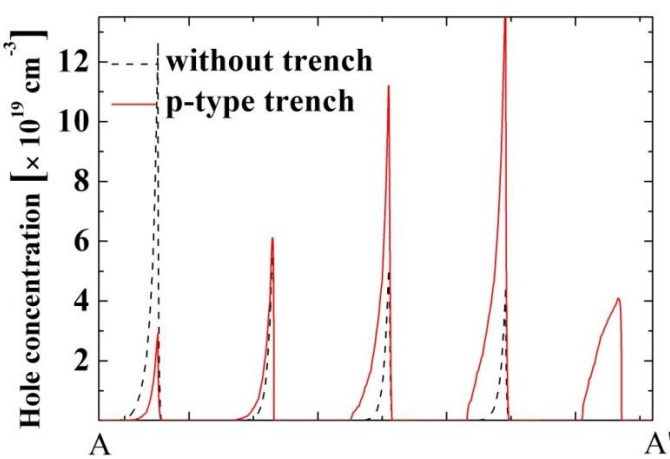

Fig. 4.3. Calculated hole concentration at current of 1 A for the conventional LED and the p-type trench LED.

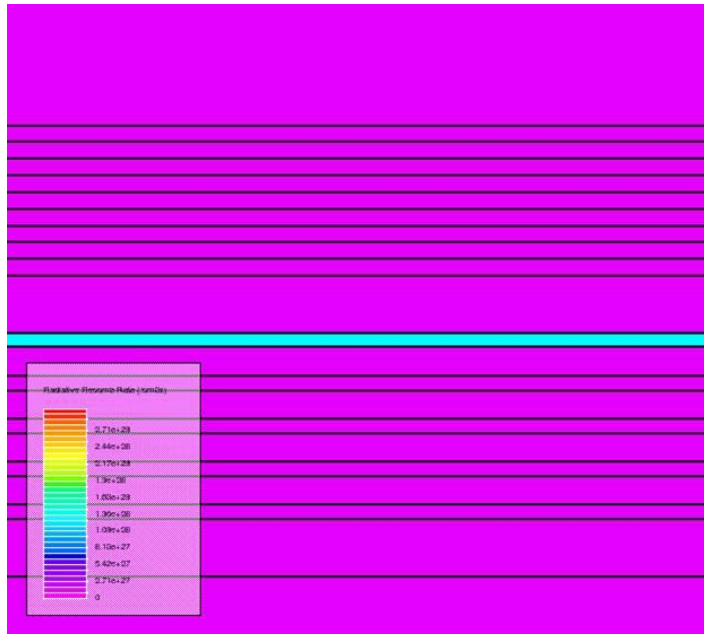

(a)

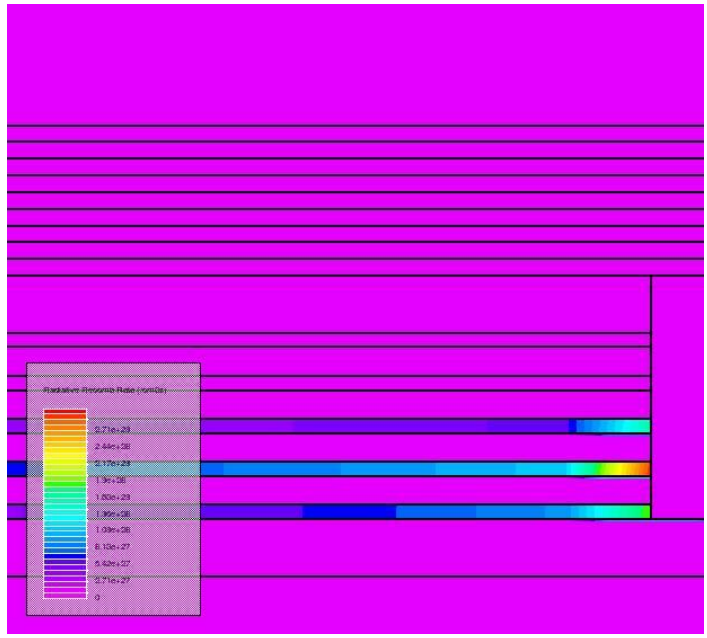

(b)

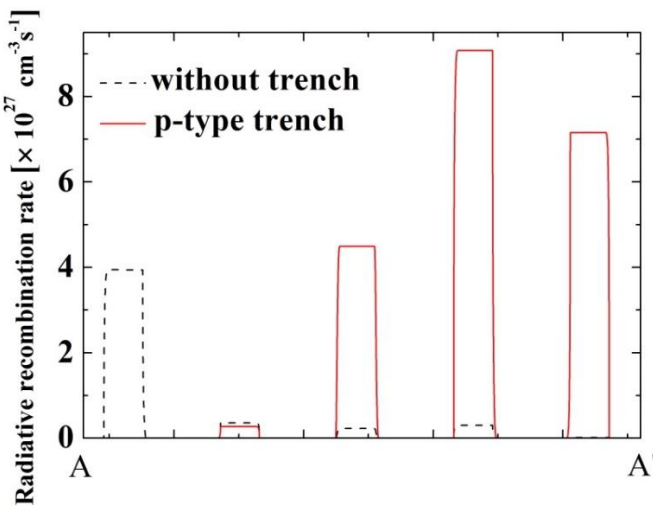

(c)

Fig. 4.4. Calculated radiative recombination rate at current of 1 A for (a) the conventional LED and (b) the p-type trench LED. (c) Radiative recombination rates cut through the A-A' line of Fig. 4.2.

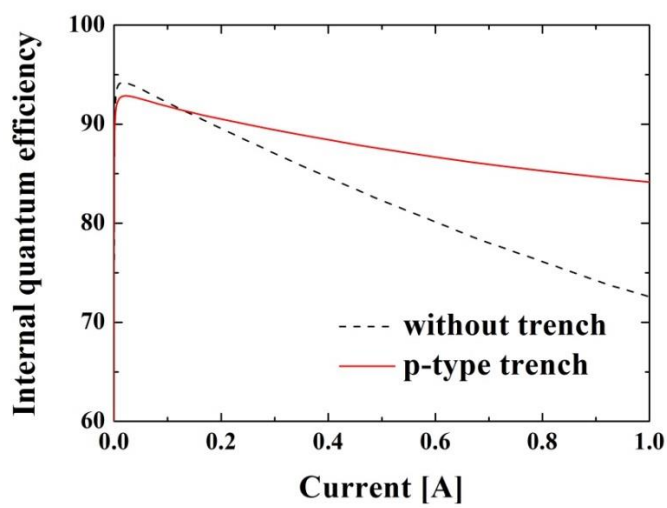

Fig. 4.5. Internal quantum efficiency of the conventional LED and the p-type trench LED.

As holes are injected and distributed through the p-type trench, it is important to determine proper physical parameters (the width of the p-type trench and the distance between the trenches) of the p-type trench (Fig. 4.6). In order to optimize these parameters, we analyzed the optical and electrical characteristics of the proposed structure when the width of the p-type trench and distance between the trenches are changed. Figure 4.7 shows how the width of the p-type trench influences the IQE of the proposed structure. As the volume of the active region is reduced and the leakage current through the p-type trench increases, the IQE of the proposed structure decreases when the width of the p-type trench increases as shown in Fig. 4.7. The change of the IQE according to the distance between the trenches is also analyzed, and the result is illustrated in Fig. 4.8. As the distance between the trenches is reduced, holes are distributed more uniformly and the IQE is improved. From these results, it can be concluded that the IQE and the light output power are improved by inserting narrower p-type trench more frequently into the MQW layer.

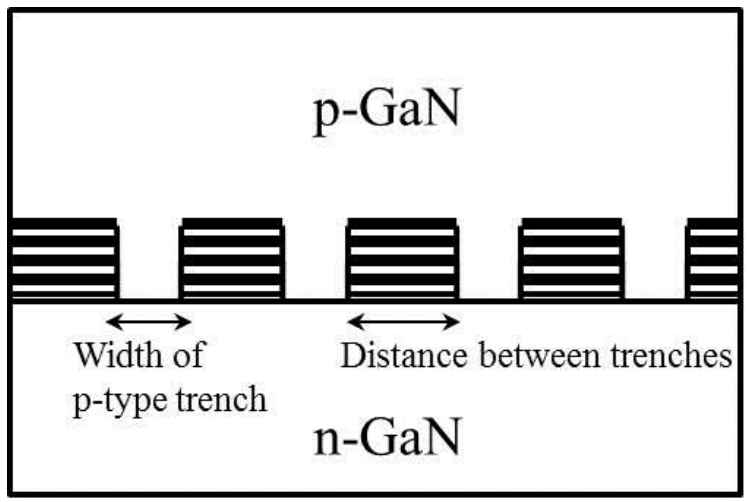

Fig. 4.6. Critical physical parameters of the p-type trench LED (the width of the p-type trench and the distance between the trenches).

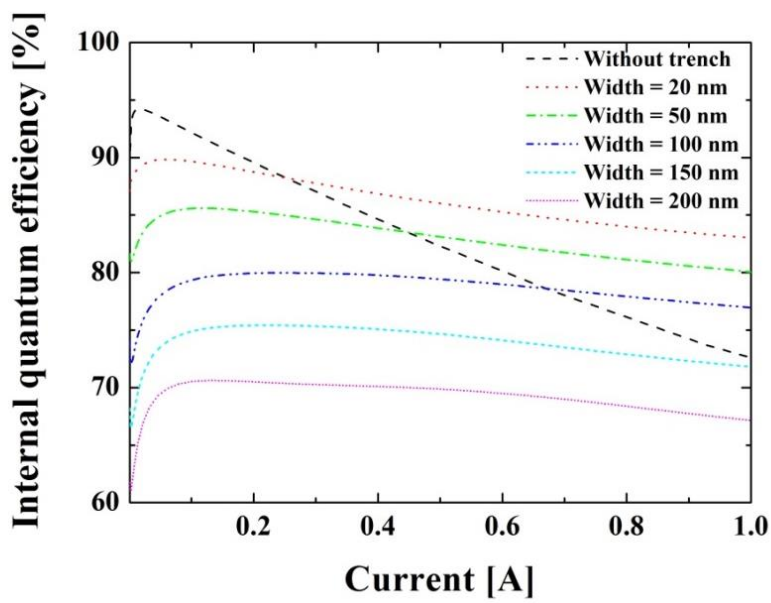

Fig. 4.7. Internal quantum efficiency of the proposed structure when the width of the p-type trench is changed.

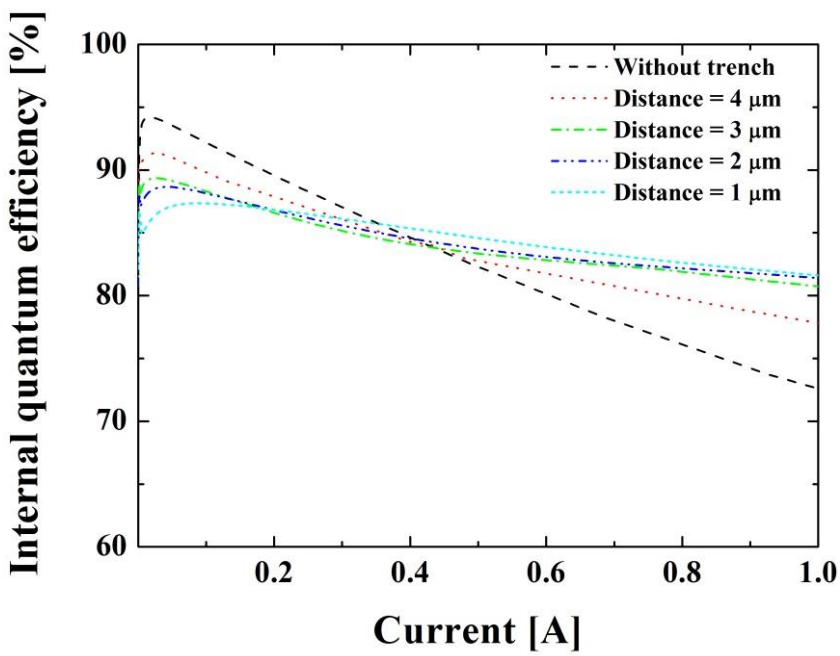

Fig. 4.8. Internal quantum efficiency of the proposed structure when the distance between the p-type trench is changed.

Figure 4.9 shows a simple fabrication method for manufacturing the proposed structure. First, n-GaN and MQW layers are grown on sapphire substrate by MOCVD process (Fig. 4.9(a)). Then, trench structures are patterned by e-beam lithography or selective wet etching process (Fig. 4.9(b)). After the trench patterning process, p-type layer is grown laterally to fill the trench region in the MQW layer (Fig. 4.9(c)) [42]. These figures indicate that the p-type trench can be easily defined by adding the trench patterning process and lateral overgrowth process.

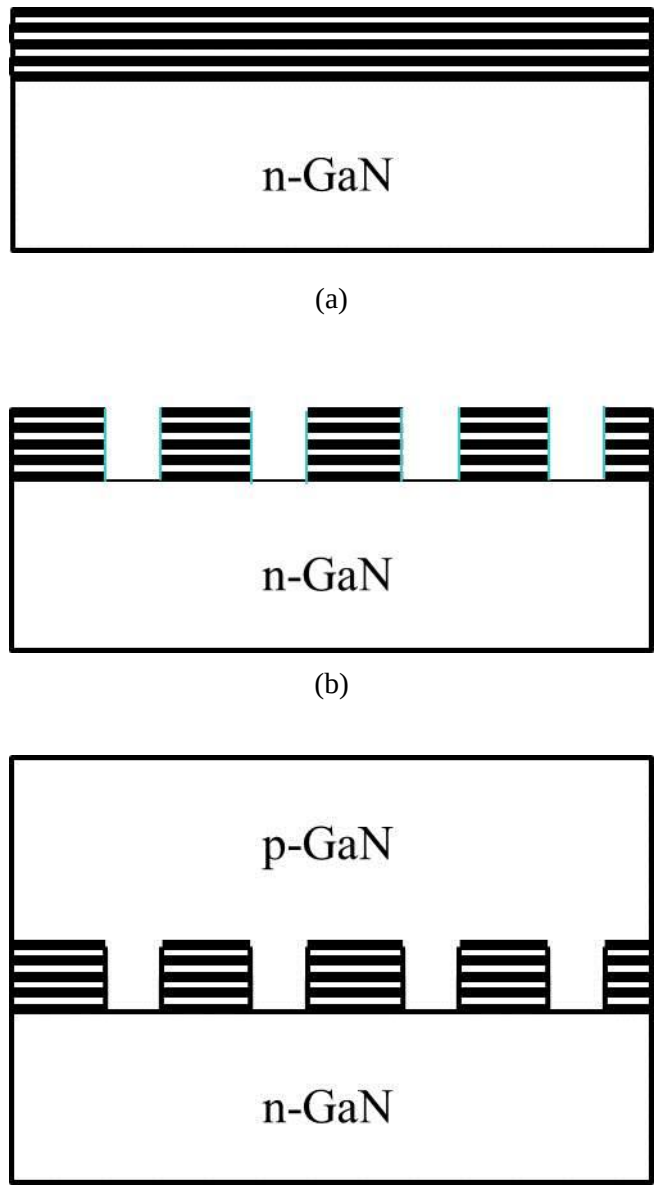

Fig. 4.9. Fabrication process for the p-type trench LED. (a) n-GaN and MQW layers are grown on sapphire substrate by MOCVD process. (b) Trench structures are patterned in by e-beam lithography or selective wet etching process. (c) p-GaN layer is filled in the trench by using lateral overgrowth process.

4.3 Trench patterning using e-beam lithography

The major fabrication processes of the trench patterning process using e-beam lithography are as follows. Epitaxial layers were grown by metal-organic chemical vapor deposition (MOCVD) on a c-plane sapphire substrate. After the growth of undoped GaN layer and n-type GaN layer, InGaN/GaN MQW layer was grown as an active region emitting blue light. The MQW layer consists of seven pairs of 3-nm-thick InGaN wells and 12-nm-thick barriers. 100-nm-thick polymethyl methacrylate (PMMA) resist was coated on the prepared sample by spin coating process, and periodic trench structures were defined by electron-beam (e-beam) lithography with an accelerating voltage of 100 keV and a beam current of 1 nA. These trench patterns were transferred into the InGaN/GaN MQW layer by inductively-coupled plasma (ICP) dry etching process using the defined PMMA layer as a hard mask. After the dry etching process, the remaining PMMA layer was removed with acetone and the samples are rinsed in deionized (DI) water.

In addition to the improved hole injection, the proposed structure has an effect on the strain relaxation and reduction of the quantum-confined stark effect (QCSE). For the continuous improvement of the efficiency in the GaN-based LEDs, it is important to reduce QCSE in multi-quantum-well (MQW) induced by polarization field [3, 43]. The polarization field in the MQW is mainly attributed to the strain caused by large lattice constant mismatch between InGaN and GaN. In order to reduce the strain and the QCSE, several solutions have been proposed and investigated, such as growing on non- or

semi-polar substrate [44-46], applying external stress [47], and patterning nanostructure MQW [48-50]. Among these methods, nanostructure patterning in the MQW has been investigated as a promising solution for reducing the stain and the QCSE. As the strain induced by lattice mismatch can be reduced with the size of the MQW, the proposed structure can increase the electron and hole wave-function overlap and radiative recombination rate. In order to analyze this effect, the wavelength and the intensity of the light emitting from the MQW are confirmed by CL measurement. Figure 4.10 shows the schematic cross-section of the prepared sample. To study the effects of the period of the trench, the period was split into four cases (200 nm, 500 nm, 1 μm, 2 μm), while the width of the trench was fixed at 50 nm. We prepared two types of the samples (square pattern structure and stripe pattern structure), and Figures 4.11(a) and (b) show the plan view scanning electron microscope (SEM) pictures of the square pattern structure and the stripe pattern structure, respectively. For an accurate comparison, all structures are close to each other and on the same wafer.

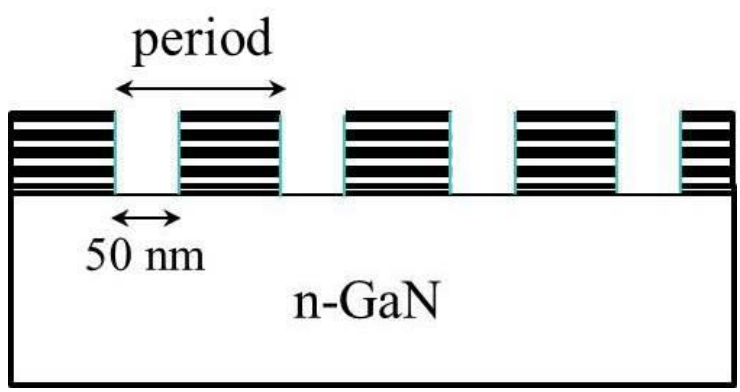

Fig. 4.10. Schematic cross-sectional view of the trench structure in the MQW.

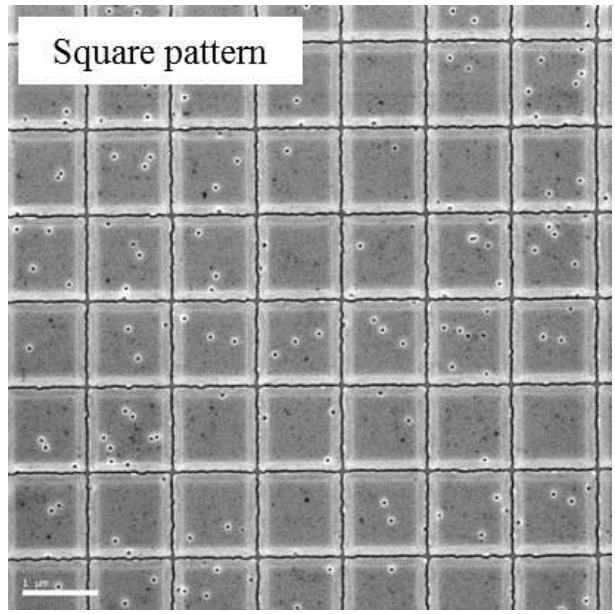

(a)

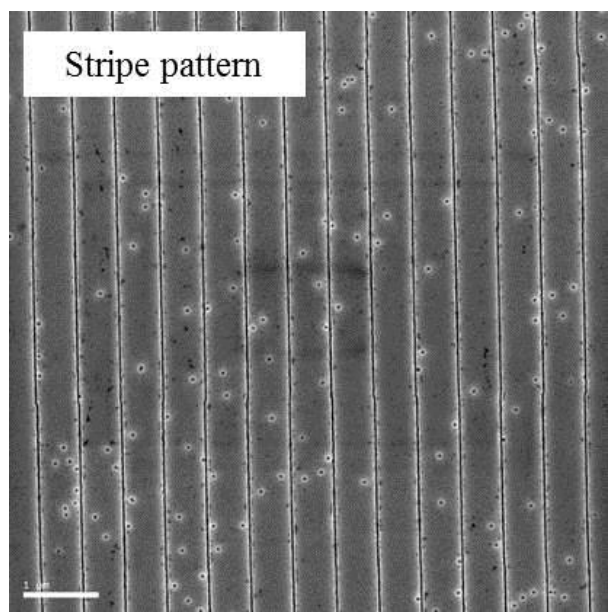

(b)

Fig. 4.11. Plan view SEM pictures of (a) the square pattern structure and (b) the stripe pattern structure.

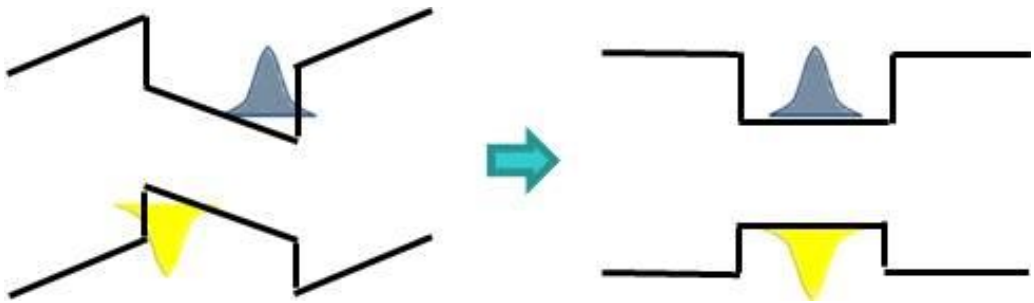

Fig. 4.12. Energy band structure in the MQW when the strain is (a) present or (b) eliminated.

In order to confirm the relaxation effects of the strain and the QCSE caused by the periodic trench patterns, the prepared samples were investigated by CL spectroscopy. When strain is present in the MQW, the polarization field induced by this strain can bend the energy band structure in the MQW as shown in Fig. 4.12(a). This band bending leads to narrowing of effective bandgap and increases the peak wavelength of emitted light. In addition, the polarization field shifts the positions of electrons and holes to the opposite side of the well, resulting in reduced wave function overlap and decreased light output intensity. In the case of the prepared samples, it is expected that the trench structures in the MQW reduce this strain effect and change the energy band structure as illustrated in Fig. 4.12(b). The peak wavelength would be blue-shifted and the light output intensity would increase since the strain will decrease as the period of trenches decreases.

Fig. 4.13(a) and Fig. 4.13(b) show measured CL spectra of the square pattern structure and the stripe pattern structure, respectively. The CL spectra were obtained for an electron energy of 5 keV and the size of scanning area (50 μm^2) remained constant. The curves with black square symbols in these figures represent CL spectra recorded from the as-grown sample without the periodic trench structure. The peak of the CL spectrum is located at the wavelength of 450 nm. By comparing the measured CL spectra of the prepared samples with that of the as-grown sample, we can confirm that the inserted trench structures change the peak wavelength and intensity of the CL spectra significantly. In order to investigate the effects of the trench structures more precisely, peak wavelength and peak intensity of the CL spectra are plotted as a function of the remaining active region (%) in Fig. 4.14(a) and Fig. 4.14(b), respectively. Fig. 4.14(a) shows that the peak wavelength of the CL spectra is blue-shifted due to the strain relaxation effect when the percentage of the remaining active region is reduced. When the remaining active region is the smallest (56.25 %), the peak wavelength shifted most (from 450 nm to 435 nm). It means that the effective bandgap of the MQW changed from 2.76 eV to 2.85 eV by the reduced QCSE. Meanwhile, the peak intensity of the CL spectra does not increase monotonically as the percentage of the remaining active region decreases (Fig. 4.14(b)).

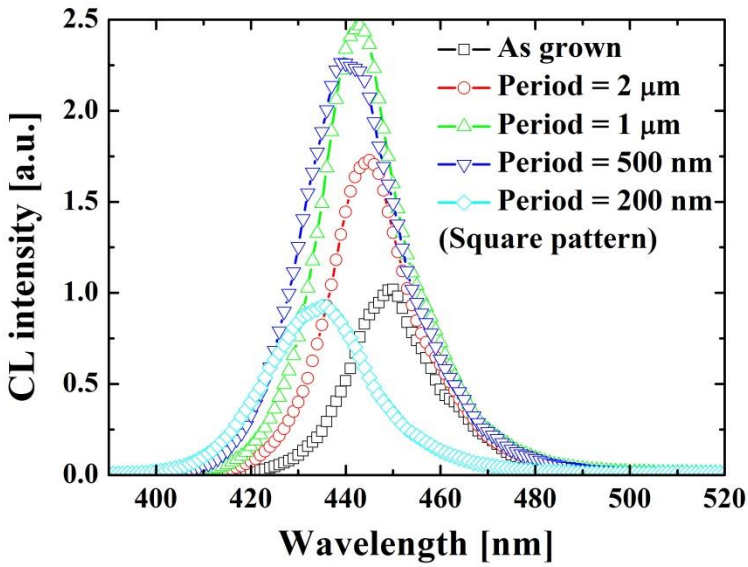

(a)

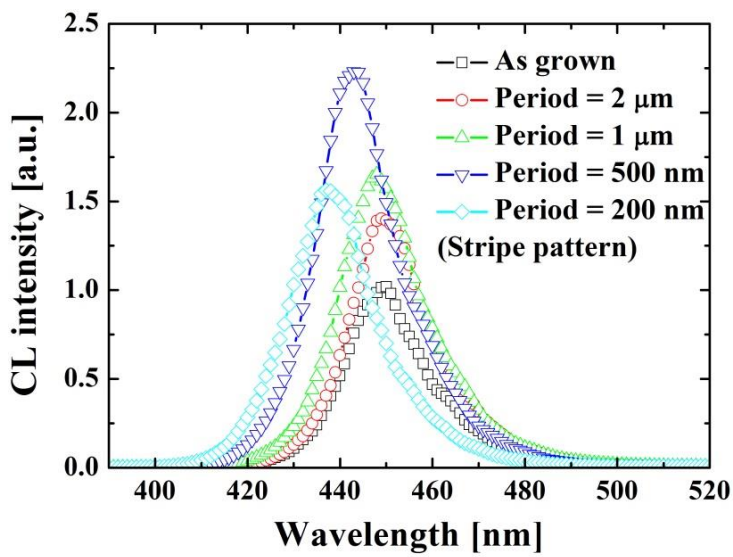

(b)

Fig. 4.13. Measured CL spectra of (a) the square pattern structure and (b) the stripe pattern structure.

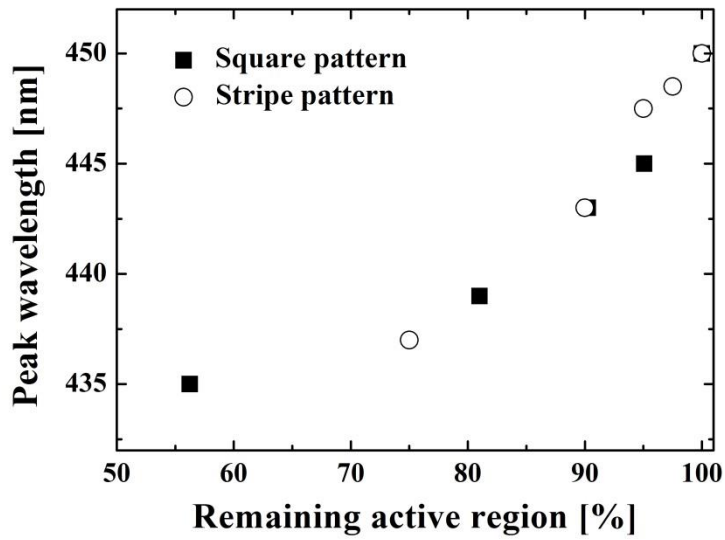

(a)

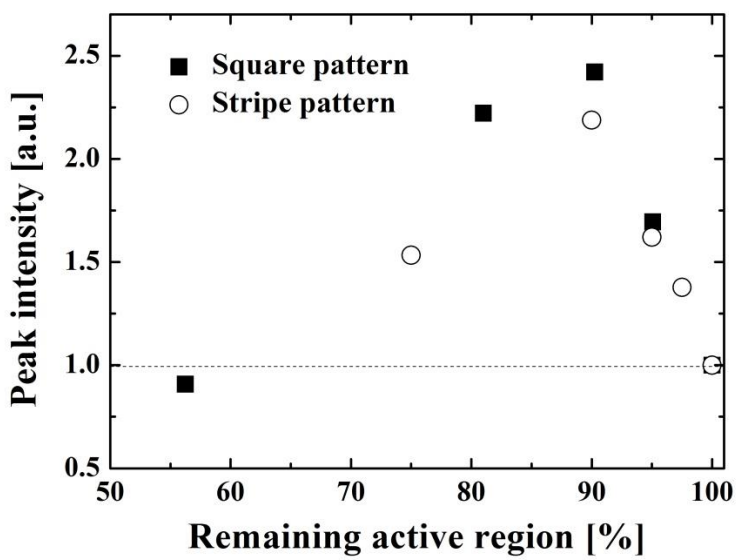

(b)

Fig. 4.14. (a) Peak wavelength and (b) peak intensity of the CL spectra plotted as a function of the remaining active region except trench region.

The peak intensity shows a maximum value at the remaining active region of 90 % and decreases as the remaining active region becomes smaller. This is because the trench structures also reduce the volume of the light emitting region while decreasing the strain and the QCSE. Rapid reduction of the peak intensity for remaining active region of less than 90 % indicates that the strain relaxation is almost complete in this condition. Consequently, in order to improve the light output intensity, it is important to maintain the proper ratio between the trench and the remaining active region. From this experiment, it is confirmed that the light output intensity can be maximized when 90 % of the active region remains.

4.4 Trench patterning using selective wet etching

In the previous chapter, the trench pattering method using e-beam lithography was introduced. However, e-beam lithography has some disadvantages like long exposure time and high fabrication cost. In order to overcome these problems of e-beam lithography, trench patterning method using selective wet etching is proposed. It is well known that threading dislocations in nitride-based materials can be selectively etched by using several etchants like NaOH-KOH eutectic melt, KOH melt, or mixture of H_2SO_4 and H_3PO_4 in various temperature conditions. This selective wet etching method has been widely used for determination of dislocation density or surface texturing to enhance the extraction efficiency of GaN-based LEDs.

In this research, the selective wet etching method was used for the trench patterning in the MQW of GaN-based LEDs. For the selective wet etching process, an etchant solution of 5 M KOH solution in ethylene glycol was used at 165°C. This process condition is based on the research of S.-I. Na et al [51]. Figure 4.15 shows the microscope image of before and after 30 min selective wet etching process.

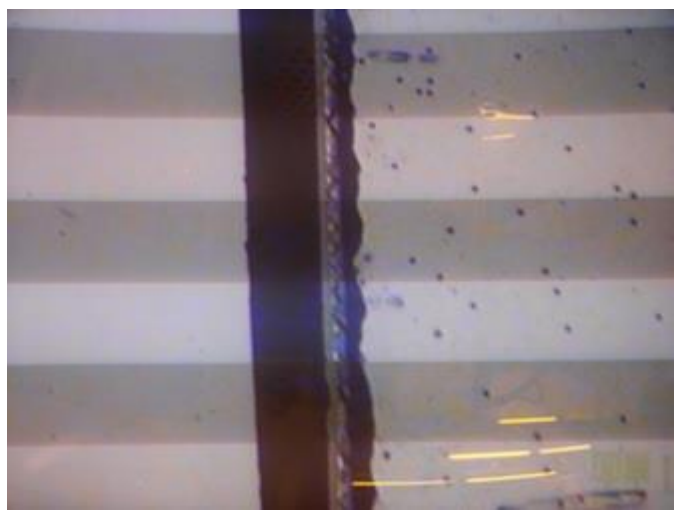

Fig. 4.15. Microscope picture of before (left) and after (right) selective wet etching.

Figure 4.16(a) and (b) show the plan view and the cross-sectional view SEM images of 30 nm selective wet etching sample, respectively. As shown in Fig. 4.7, the IQE of the proposed structure increases when the width of the p-type trench decreases. On the basis of these experiments and simulation results, selective wet etching time for main samples was split into three cases (4, 5, 6 min).

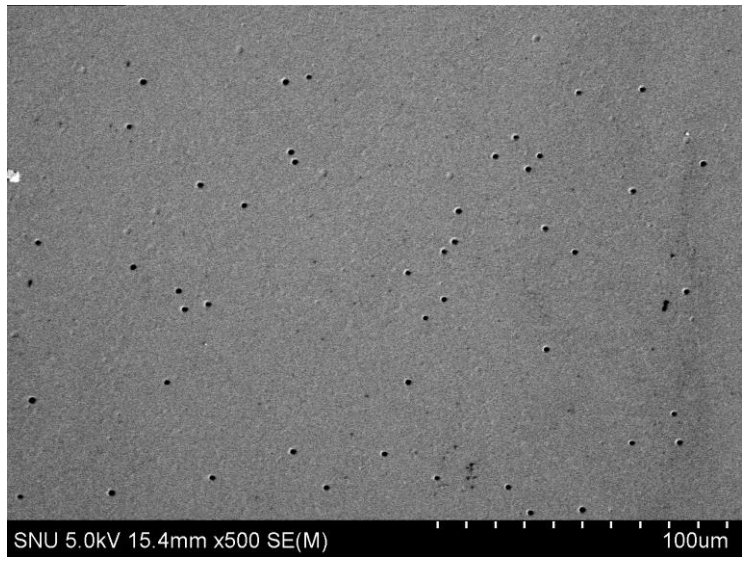

(a)

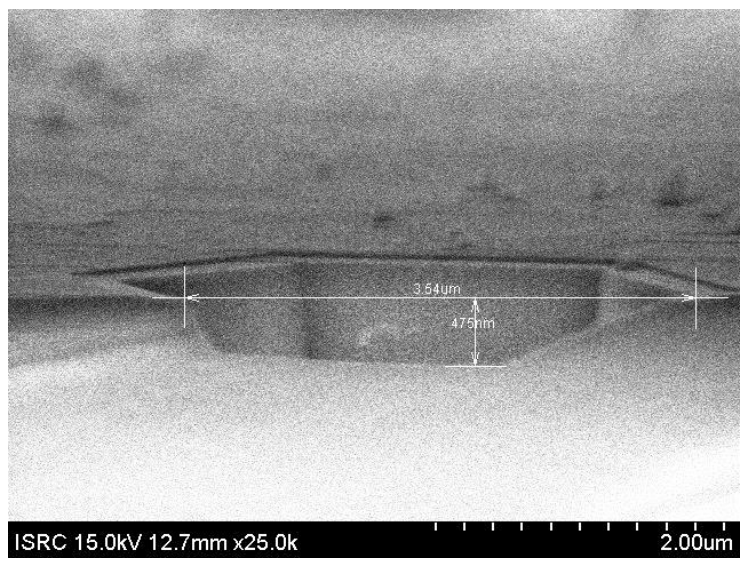

(b)

Fig. 4.16. (a) Plan view and (b) cross-sectional view SEM pictures of selective wet etching sample for 30 min etching time.

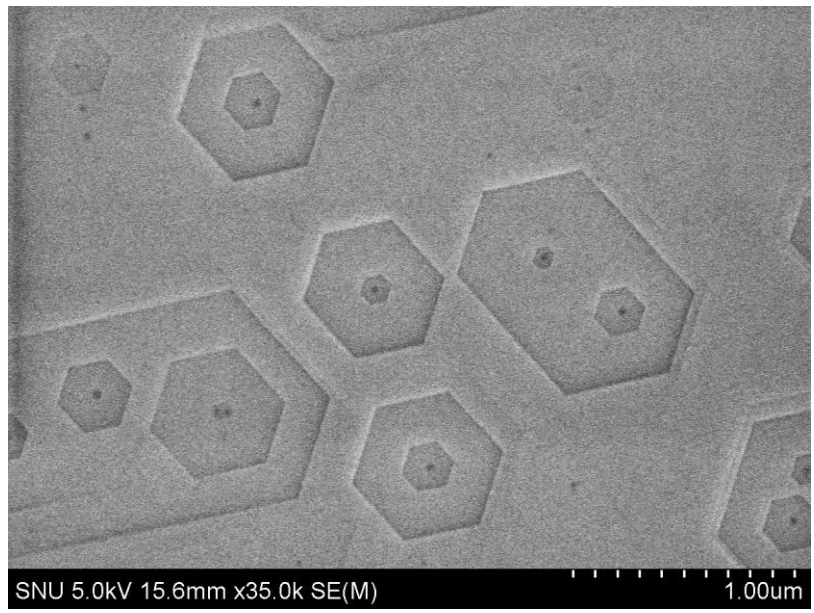

(a)

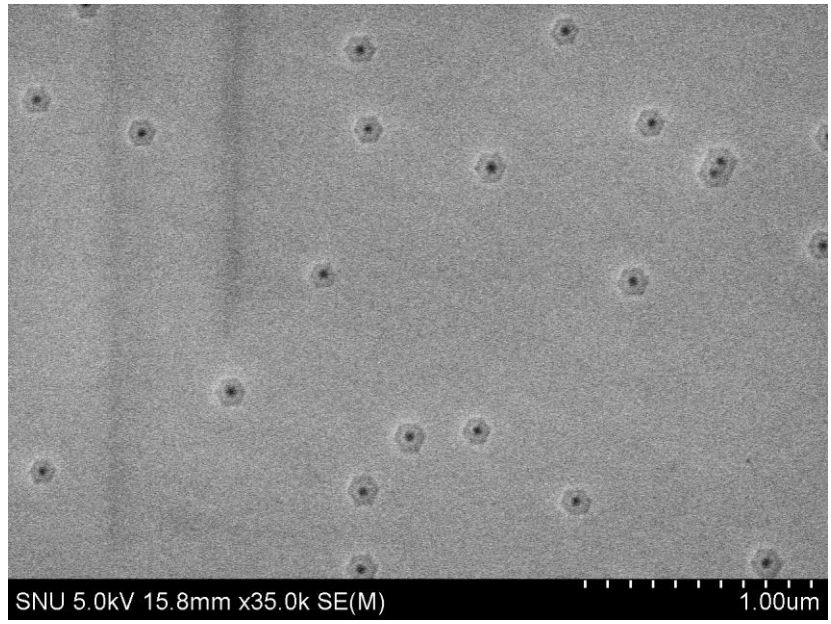

(b)

Fig. 4.17. Plan view SEM pictures of selective wet etching sample for (a) 15 min etching time and (b) 5 min etching

4.5 Measurement results

After the trench patterning process using e-beam lithography or selective wet etching, p-type layer is grown laterally to fill the trench region in the MQW layer at 950°C and at a pressure of 200 Torr. ITO layer is used for current spreading and Cr/Ni metal contact layer is deposited by e-beam evaporation. Figure 4.18 shows the plan view microscope image of the fabricated GaN-based LED. Cross-sectional views of the p-type trench are captured by tunneling electron microscope (TEM) as shown in Fig. 4.19(a) and (b). It can be confirmed that the p-type trench is successfully fabricated by e-beam lithography and re-growth process.

At first, electrical and optical characteristics of the proposed structure using e-beam lithography are analyzed. As shown in Fig. 4.20, forward current of the proposed samples is higher because of the improved hole injection through the p-type trench. Reverse current of the proposed samples is also increased because of the leakage current through the p-type trench as shown in Fig. 4. 21. Figure 4.22 and 4.23 show the light output power and efficiency of the proposed structure using e-beam lithography and the conventional structure. Because the proposed structure has effects on hole distribution in the MQW and strain relaxation, the light output power and efficiency of the proposed structure are much improved. By comparing the measured (electro-luminescence) EL spectra of the proposed structure with that of the conventional structure in Fig. 4.24, it is also confirmed that the p-type trench structure changes the peak wavelength and improves the intensity of the EL spectra significantly by strain relaxation.

Fig. 4.18. Microscope picture of fabricated GaN-based LEDs.

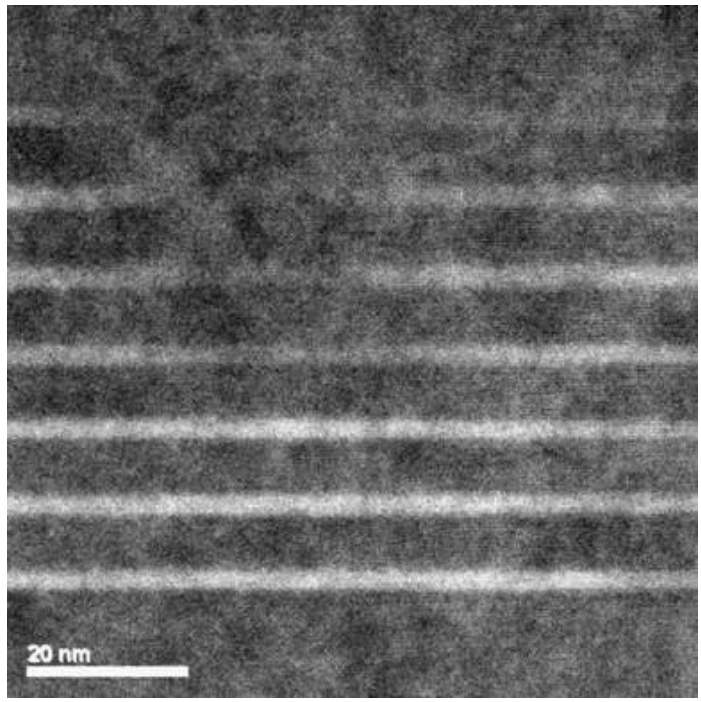

(a).

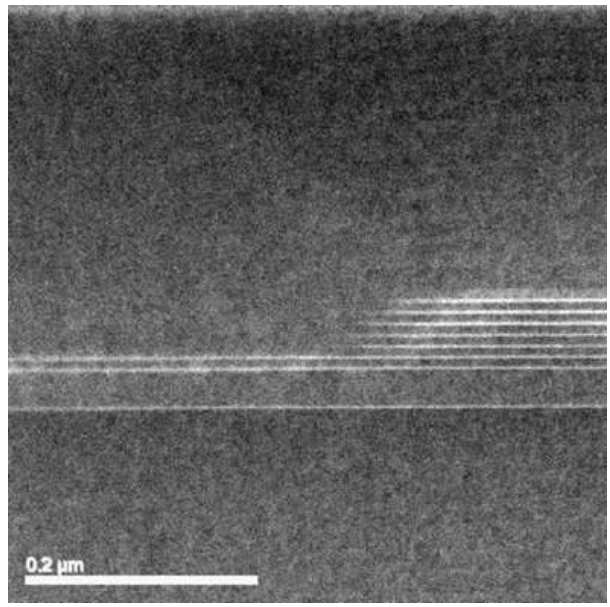

(b)

Fig. 4.19 Cross-sectional view TEM images of (a) 50 nm target trench structure and (b) 3 μm target trench structure

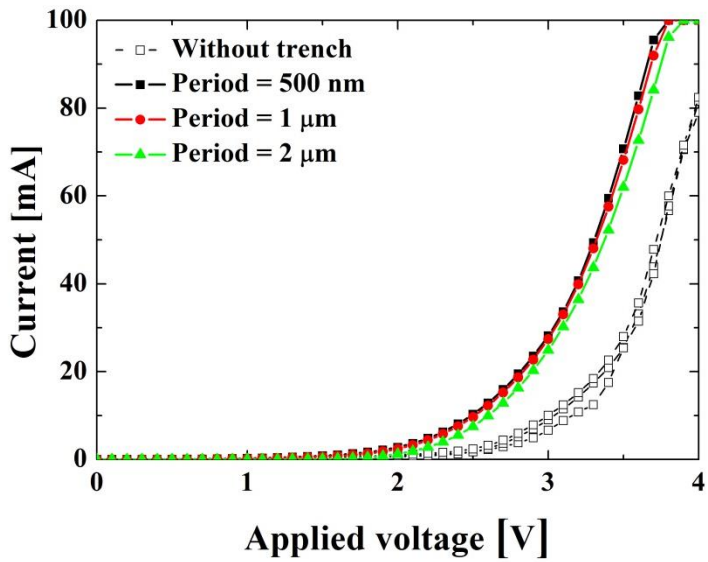

Fig. 4.20. Forward current characteristics of the p-type trench structure using e-beam lithography and the conventional structure.

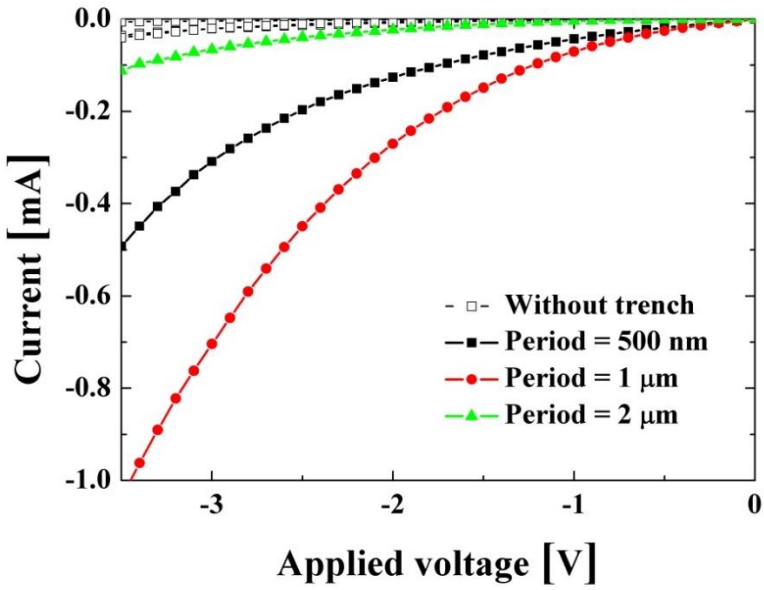

Fig. 4.21. Reverse current characteristics of the p-type trench structure using e-beam lithography and the conventional structure.

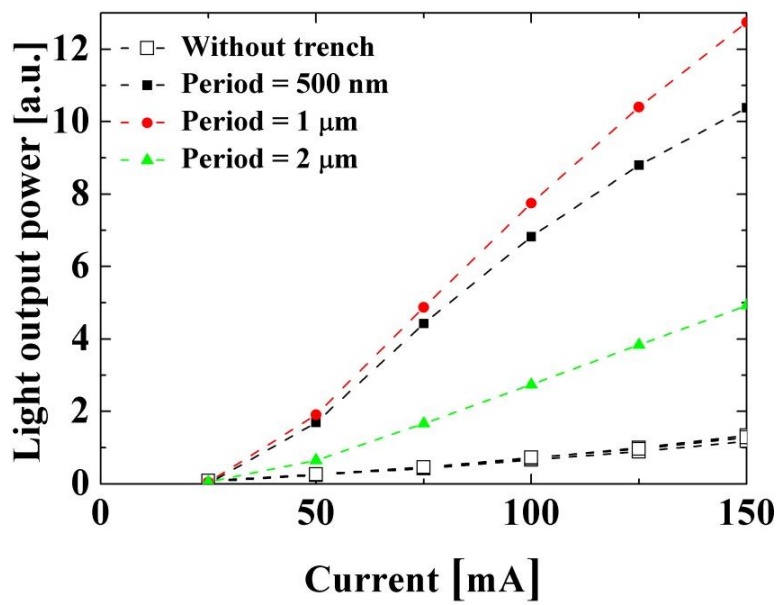

Fig. 4.22 Light output power of the p-type trench structure using e-beam lithography and the conventional structure.

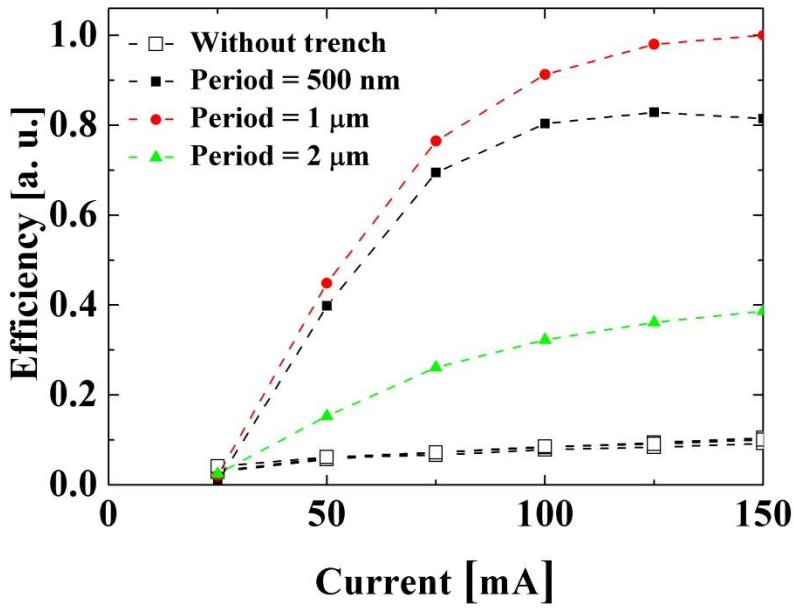

Fig. 4.23 Efficiency of the p-type trench structure using e-beam lithography and the conventional structure.

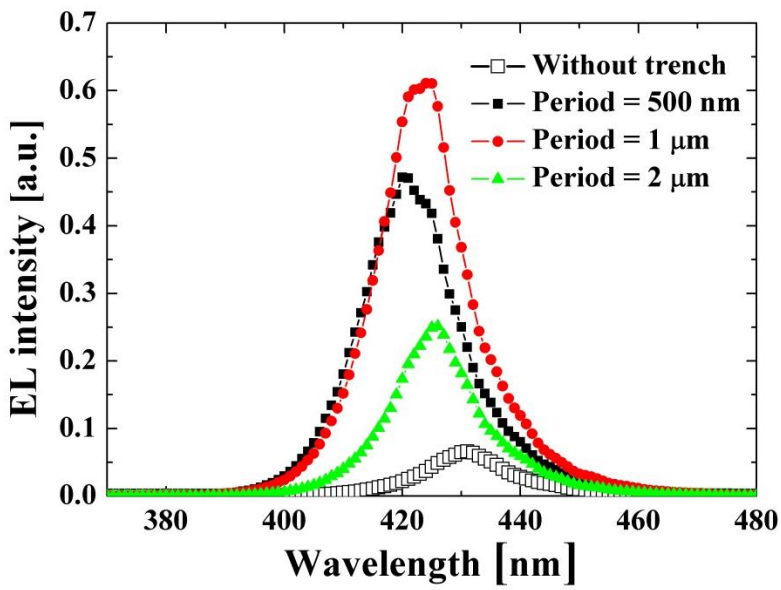

Fig. 4.24 Electro-luminescence (EL) of the p-type trench structure using e-beam lithography and the conventional structure.

For a more detailed analysis, recombination coefficients and IQE of 1 μm period p-type trench structure are extracted. Figure 4.25 shows the measured transient characteristics of the light output power when 100-mA current pulse is applied. By fitting the transient characteristics to Eq. (2.1b) in Chapter 2, the recombination coefficients are extracted and compared to the data of the conventional structure analyzed in Chapter 2 (Table 4.1). The IQE of the p-type trench structure is also calculated with the recombination coefficients extracted by transient measurement (Figure 4.26). As shown in Table 4.1, radiative recombination coefficient *B* increases and coefficient *C* causing efficiency droop decreases compared to the conventional structure. In contrast, SRH recombination coefficient *A* of the p-type trench structure is severely increased. It is assumed that the trap density is increased during the p-type trench patterning process.

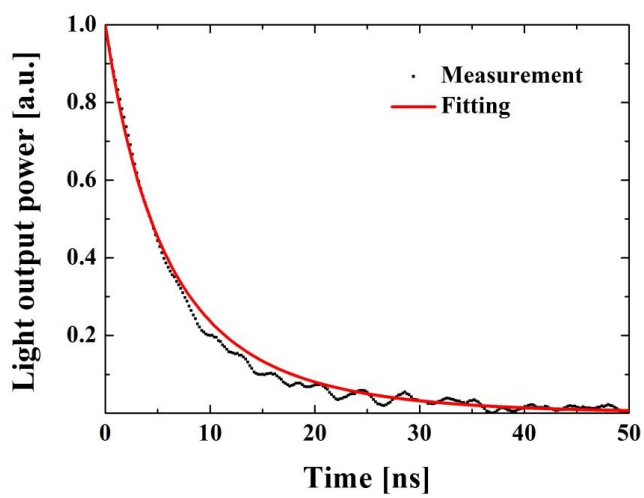

Fig. 4.25. Measured transient characteristics of the light output power of the 1 μm period p-type trench structure.

Table 4.1. Calculated recombination coefficients of the1 μm period p-type trench structure and the conventional structure.

	A (s^{-1})	B ($cm^3 s^{-1}$)	C ($cm^6 s^{-1}$)
Conventional structure (Measured in Chapter 2)	8.4×10^{6}	1.3×10^{-11}	1.9×10^{-31}
1 μm period p-type trench structure	5.0×10^{7}	2.1×10^{-11}	1.7×10^{-31}

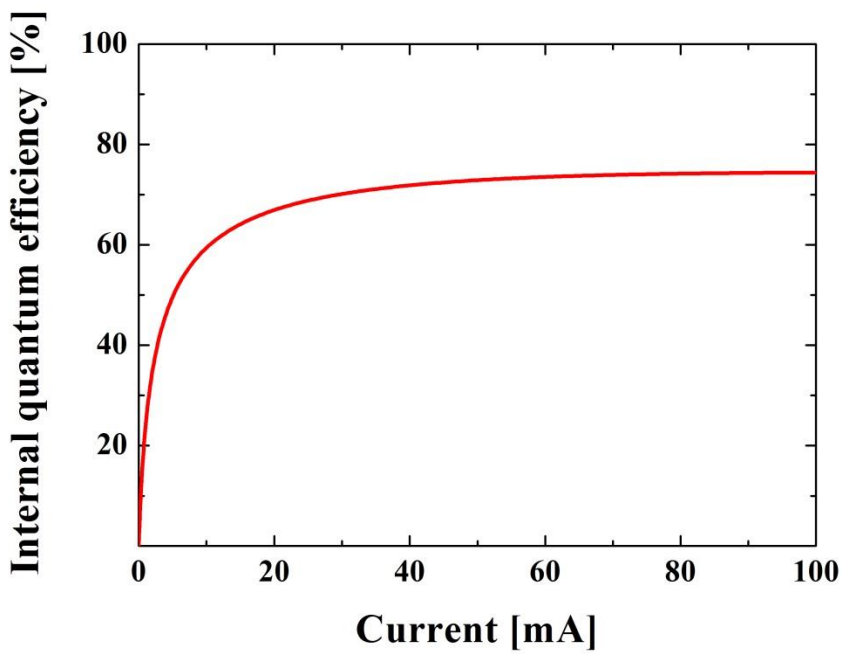

Fig. 4.26. Calculated IQE of the 1 μm period p-type trench structure.

Electrical and optical characteristics of the proposed structure using selective wet etching are also analyzed. Figure 4.27 and 4.28 show the light output power and efficiency of the proposed structure using selective wet etching and the conventional structure. Like e-beam lithography samples, selective wet etching samples also show higher light output power and efficiency than the conventional structure because the hole distribution in the MQW is improve by the p-type trench. However, the peak wavelength of the EL spectra is barely changed as shown in Fig. 29. From this result, it can be confirmed that the light output power improvement of the selective wet etching sample is originated from the better hole injection, not from the strain relaxation effect.

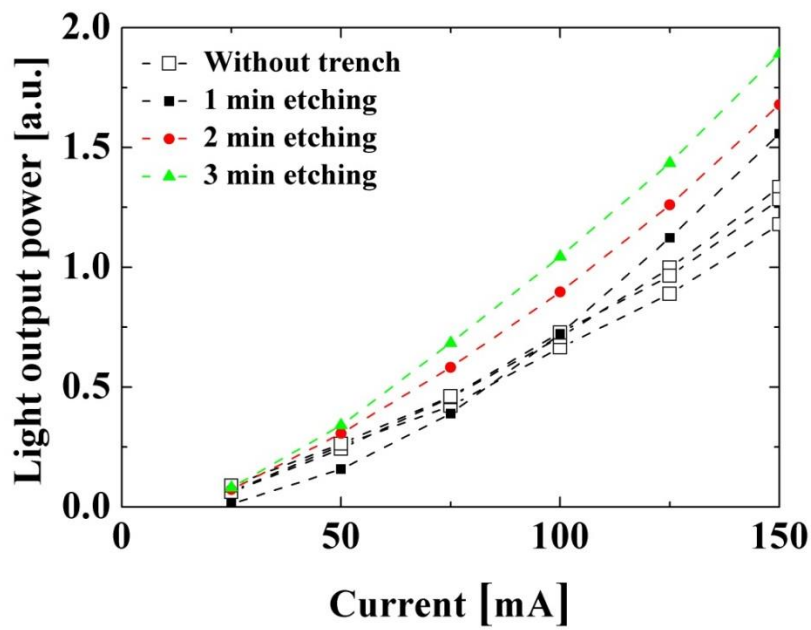

Fig. 4.27. Light output power of the p-type trench structure using selective wet etching and the conventional structure.

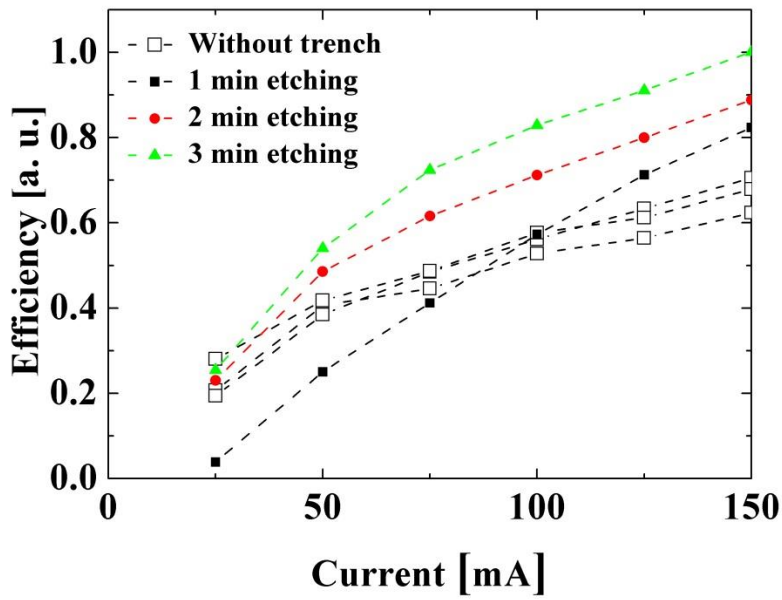

Fig. 4.28. Efficiency of the p-type trench structure using selective wet etching and the conventional structure.

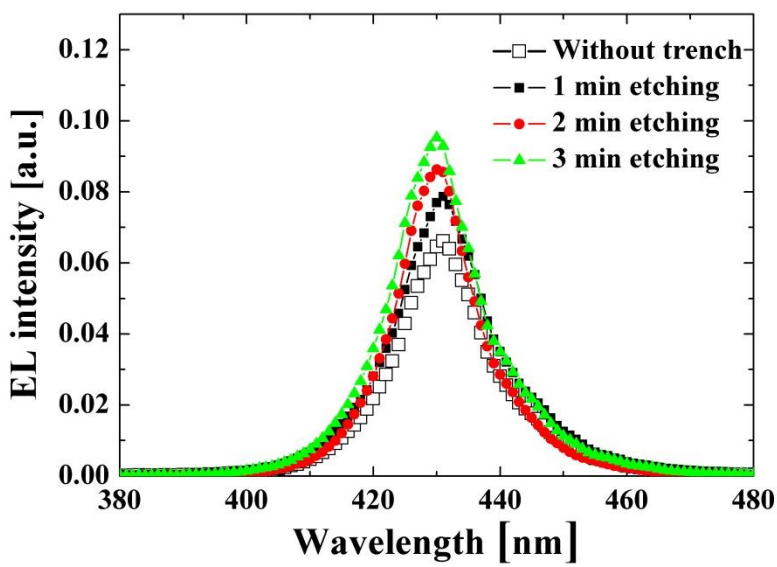

Fig. 4.29 EL of the p-type trench structure using selective wet etching and the conventional structure.

Chapter 5

Conclusions

A simple and rapid method is introduced to extract recombination coefficients and IQE by using transient analysis of GaN-based LED. A modified rate equation model of GaN-based LEDs is also proposed considering the effective volume of the active region. It is confirmed that polarization charge, quantum well barriers, and high current density reduce the effective volume and cause the efficiency droop. By analyzing the transient characteristics of the LED sample, it is confirmed that the proposed model can extract the recombination coefficients and IQE of GaN-based LEDs correctly.

An abnormal increase in the current of GaN-based LEDs is analyzed and a trap activation energy of 0.30 eV is extracted by current-transient methodology. It is confirmed that this activation energy is consistent with the peak energy of the CL spectrum. In addition, the relationship between the current increase and the trapping process is analyzed by a TCAD simulation. It is also confirmed that this trapping process reduces the internal quantum efficiency and light output power owing to the increased SRH recombination rate.

In addition, p-type trench LED is proposed to inject hole into the MQW uniformly and improve the IQE at high current density. Through a TCAD simulation, it is confirmed that the hole distribution in the MQW is improved by inserting p-type trench into the MQW layer. Because of improved hole injection and distribution through the p-type trench, the IQE of the proposed structure is significantly increased. Through CL measurements, it is also confirmed that the proposed structure has a significant effect on strain relaxation and the consequent reduction in quantum confined stark effect. In addition, two simple fabrication methods using e-beam lithography and selective wet etching for manufacturing the proposed structure are also suggested. From the analysis of the electrical and optical characteristics of the manufactured GaN-based LEDs, it is confirmed that the proposed structure using e-beam lithography or selective wet etching shows improved forward current characteristics and light output power.

Bibliography

[1] H. Jia, L. Guo, W. Wang, and H. Chen, "Recent Progress in GaN-Based Light-Emitting Diodes," Advanced Materials, vol. 21, no. 45, pp. 4641-4646, 2009.

[2] M. Koike, N. Shibata, H. Kato, and Y. Takahashi, "Development of high efficiency GaN-based multiquantum-well light-emitting diodes and their applications," Selected Topics in Quantum Electronics, IEEE Journal of, vol. 8, no. 2, pp. 271-277, 2002.

[3] A. David and M. J. Grundmann, "Influence of polarization fields on carrier lifetime and recombination rates in InGaN-based light-emitting diodes," Applied Physics Letters, vol. 97, no. 3, pp. 033501-033501-3, 2010.

[4] P. T. N. Hieu, K. Cui, S. F. Zhang, M. Djavid, A. Korinek, G. A. Botton, et al., "Controlling Electron Overflow in Phosphor-Free InGaN/GaN Nanowire White Light-Emitting Diodes," Nano Letters, vol. 12, no. 3, pp. 1317-1323, Mar 2012.

[5] E. Kioupakis, P. Rinke, K. T. Delaney, and C. G. Van de Walle, "Indirect Auger recombination as a cause of efficiency droop in nitride light-emitting diodes,"

Applied Physics Letters, vol. 98, no. 16, pp. 161107-161107-3, 2011.

[6] Q. M. Li, K. R. Westlake, M. H. Crawford, S. R. Lee, D. D. Koleske, J. J. Figiel, et al., "Optical performance of top-down fabricated InGaN/GaN nanorod light emitting diode arrays," Optics Express, vol. 19, no. 25, pp. 25528-25534, Dec 5 2011.

[7] S. Nakamura, N. Senoh, N. Iwasa, and S. I. Nagahama, "High-Brightness Ingan Blue, Green and Yellow Light-Emitting-Diodes with Quantum-Well Structures," Japanese Journal of Applied Physics Part 2-Letters, vol. 34, no. 7A, pp. L797-L799, Jul 1 1995.

[8] H. Y. Ryu and J. I. Shim, "Effect of current spreading on the efficiency droop of InGaN light-emitting diodes," Optics Express, vol. 19, no. 4, pp. 2886-2894, Feb 14 2011.

[9] I. P. Seetoh, C. B. Soh, L. Zhang, K. H. P. Tung, E. A. Fitzgerald, and S. J. Chua, "Improvement in the internal quantum efficiency of InN grown over nanoporous GaN by the reduction of Shockley-Read-Hall recombination centers," Applied Physics Letters, vol. 103, no. 12, p. 121903, 2013.

[10] Y.-R. Wu, C. Chiu, C.-Y. Chang, P. Yu, and H.-C. Kuo, "Size-dependent strain relaxation and optical characteristics of InGaN/GaN nanorod LEDs," Selected Topics in Quantum Electronics, IEEE Journal of, vol. 15, no. 4, pp. 1226-1233, 2009.

[11] J. Cho, E. F. Schubert, and J. K. Kim, "Efficiency droop in light-emitting diodes:

Challenges and countermeasures," Laser & Photonics Reviews, 2012.

[12] J. Piprek, "Efficiency droop in nitride-based light-emitting diodes," Physica Status Solidi a-Applications and Materials Science, vol. 207, no. 10, pp. 2217-2225, Oct 2010.

[13] M. F. Schubert, J. Xu, J. K. Kim, E. F. Schubert, M. H. Kim, S. Yoon, et al., "Polarization-matched GaInN/ AlGaInN multi-quantum-well light-emitting diodes with reduced efficiency droop," Applied Physics Letters, vol. 93, p. 041102, 2008.

[14] J. Xie, X. Ni, Q. Fan, R. Shimada, U. Ozgur, and H. Morkoc, "On the efficiency droop in InGaN multiple quantum well blue light emitting diodes and its reduction with p-doped quantum well barriers," Applied Physics Letters, vol. 93, no. 12, pp. 121107-3, 09/22/ 2008.

[15] S.-H. Han, D.-Y. Lee, S.-J. Lee, C.-Y. Cho, M.-K. Kwon, S. Lee, et al., "Effect of electron blocking layer on efficiency droop in InGaN/GaN multiple quantum well light-emitting diodes," Applied Physics Letters, vol. 94, no. 23, pp. 231123-231123-3, 2009.

[16] J. Hader, J. V. Moloney, and S. W. Koch, "Density-activated defect recombination as a possible explanation for the efficiency droop in GaN-based diodes," Applied Physics Letters, vol. 96, no. 22, pp. 221106-3, 05/31/ 2010.

[17] V. K. Malyutenko, S. S. Bolgov, and A. D. Podoltsev, "Current crowding effect on the ideality factor and efficiency droop in blue lateral InGaN/GaN light

emitting diodes," Applied Physics Letters, vol. 97, no. 25, pp. 251110-3, 12/20/ 2010.

[18] Q. Dai, Q. F. Shan, J. Wang, S. Chhajed, J. Cho, E. F. Schubert, et al., "Carrier recombination mechanisms and efficiency droop in GaInN/GaN light-emitting diodes," Applied Physics Letters, vol. 97, no. 13, Sep 27 2010.

[19] N. Gardner, G. Muller, Y. Shen, G. Chen, S. Watanabe, W. Gotz, et al., "Blue-emitting InGaN–GaN double-heterostructure light-emitting diodes reaching maximum quantum efficiency above 200," Applied Physics Letters, vol. 91, no. 24, pp. 243506-243506-3, 2007.

[20] W. Guo, M. Zhang, P. Bhattacharya, and J. Heo, "Auger Recombination in III-Nitride Nanowires and Its Effect on Nanowire Light-Emitting Diode Characteristics," Nano Letters, vol. 11, no. 4, pp. 1434-1438, Apr 2011.

[21] G. B. Lin, D. Meyaard, J. Cho, E. F. Schubert, H. Shim, and C. Sone, "Analytic model for the efficiency droop in semiconductors with asymmetric carrier-transport properties based on drift-induced reduction of injection efficiency," Applied Physics Letters, vol. 100, no. 16, Apr 16 2012.

[22] S. D. Lester, F. A. Ponce, M. G. Craford, and D. A. Steigerwald, "High dislocation densities in high efficiency GaN-based light-emitting diodes," Applied Physics Letters, vol. 66, no. 10, pp. 1249-1251, 1995.

[23] M. Albrecht, H. Strunk, J. Weyher, I. Grzegory, S. Porowski, and T. Wosinski, "Carrier recombination at single dislocations in GaN measured by

cathodoluminescence in a transmission electron microscope," Journal of applied physics, vol. 92, no. 4, pp. 2000-2005, 2002.

[24] A. Hangleiter, F. Hitzel, C. Netzel, D. Fuhrmann, U. Rossow, G. Ade, et al., "Suppression of Nonradiative Recombination by V-Shaped Pits in GaInN/GaN Quantum Wells Produces a Large Increase in the Light Emission Efficiency," Physical Review Letters, vol. 95, no. 12, p. 127402, 09/14/ 2005.

[25] M. F. Schubert, S. Chhajed, J. K. Kim, E. F. Schubert, D. D. Koleske, M. H. Crawford, et al., "Effect of dislocation density on efficiency droop in GaInN⁄GaN light-emitting diodes," Applied Physics Letters, vol. 91, no. 23, pp. -, 2007.

[26] J. Hader, J. V. Moloney, and S. W. Koch, "Temperature-dependence of the internal efficiency droop in GaN-based diodes," Applied Physics Letters, vol. 99, no. 18, pp. -, 2011.

[27] B. Santic, "On the hole effective mass and the free hole statistics in wurtzite GaN," Semiconductor science and technology, vol. 18, no. 4, p. 219, 2003.

[28] K. Kumakura, T. Makimoto, and N. Kobayashi, "Mg-acceptor activation mechanism and transport characteristics in p-type InGaN grown by metalorganic vapor phase epitaxy," Journal of applied physics, vol. 93, no. 6, pp. 3370-3375, 2003.

[29] H.-Y. Ryu, D.-S. Shin, and J.-I. Shim, "Analysis of efficiency droop in nitride light-emitting diodes by the reduced effective volume of InGaN active

material," Applied Physics Letters, vol. 100, no. 13, pp. 131109-131109-4, 2012.

[30] I. Vurgaftman and J. Meyer, "Band parameters for nitrogen-containing semiconductors," Journal of Applied Physics, vol. 94, no. 6, pp. 3675-3696, 2003.

[31] J. Piprek, Semiconductor optoelectronic devices: introduction to physics and simulation: Access Online via Elsevier, 2003.

[32] A. U. s. Manual, "Device simulation software," SILVACO International, Santa Clara, CA, vol. 95054, p. 20, 2008.

[33] Q. Dai, Q. Shan, J. Cho, E. F. Schubert, M. H. Crawford, D. D. Koleske, et al., "On the symmetry of efficiency-versus-carrier-concentration curves in GaInN/GaN light-emitting diodes and relation to droop-causing mechanisms," Applied Physics Letters, vol. 98, no. 3, pp. 033506-033506-3, 2011.

[34] M. S. Ferdous, X. Wang, M. N. Fairchild, and S. D. Hersee, "Effect of threading defects on InGaN/GaN multiple quantum well light emitting diodes," Applied Physics Letters, vol. 91, no. 23, pp. -, 2007.

[35] J. Joh and J. A. del Alamo, "Impact of electrical degradation on trapping characteristics of GaN high electron mobility transistors," in Electron Devices Meeting, 2008. IEDM 2008. IEEE International, 2008, pp. 1-4.

[36] J. Joh and J. A. Del Alamo, "A current-transient methodology for trap analysis for GaN high electron mobility transistors," Electron Devices, IEEE Transactions on, vol. 58, no. 1, pp. 132-140, 2011.

[37] C. Soh, S. Chua, H. Lim, D. Chi, S. Tripathy, and W. Liu, "Assignment of deep levels causing yellow luminescence in GaN," Journal of applied physics, vol. 96, no. 3, pp. 1341-1347, 2004.

[38] A. Armstrong, T. A. Henry, D. D. Koleske, M. H. Crawford, K. R. Westlake, and S. R. Lee, "Dependence of radiative efficiency and deep level defect incorporation on threading dislocation density for InGaN/GaN light emitting diodes," Applied Physics Letters, vol. 101, no. 16, pp. 162102-162102-4, 2012.

[39] A. David, M. J. Grundmann, J. F. Kaeding, N. F. Gardner, T. G. Mihopoulos, and M. R. Krames, "Carrier distribution in (0001) InGaN/ GaN multiple quantum well light-emitting diodes," Applied Physics Letters, vol. 92, p. 053502, 2008.

[40] J. P. Ibbetson, P. T. Fini, K. D. Ness, S. P. DenBaars, J. S. Speck, and U. K. Mishra, "Polarization effects, surface states, and the source of electrons in AlGaN/GaN heterostructure field effect transistors," Applied Physics Letters, vol. 77, no. 2, pp. 250-252, 2000.

[41] K. Yang, J. R. East, and G. I. Haddad, "Numerical modeling of abrupt heterojunctions using a thermionic-field emission boundary condition," Solid-State Electronics, vol. 36, no. 3, pp. 321-330, 3// 1993.

[42] N. P. Kobayashi, J. T. Kobayashi, X. Zhang, P. D. Dapkus, and D. H. Rich, "Epitaxial lateral overgrowth of GaN over <equation>AlO_x</equation> surface formed on Si

substrate," Applied Physics Letters, vol. 74, no. 19, pp. 2836-2838, 1999.

[43] H. Gotoh, T. Tawara, Y. Kobayashi, N. Kobayashi, and T. Saitoh, "Piezoelectric effects on photoluminescence properties in 10-nm-thick InGaN quantum wells," Applied physics letters, vol. 83, no. 23, pp. 4791-4793, 2003.

[44] Y.-D. Lin, A. Chakraborty, S. Brinkley, H. C. Kuo, T. Melo, K. Fujito, et al., "Characterization of blue-green m-plane InGaN light emitting diodes," Applied Physics Letters, vol. 94, no. 26, p. 261108, 2009.

[45] H. Masui, S. Nakamura, S. P. DenBaars, and U. K. Mishra, "Nonpolar and semipolar III-nitride light-emitting diodes: achievements and challenges," Electron Devices, IEEE Transactions on, vol. 57, no. 1, pp. 88-100, 2010.

[46] H. Zhong, A. Tyagi, N. N. Fellows, F. Wu, R. B. Chung, M. Saito, et al., "High power and high efficiency blue light emitting diode on freestanding semipolar (10 1 1) bulk GaN substrate," Applied physics letters, vol. 90, no. 23, pp. 233504-233504-3, 2007.

[47] J. H. Son and J.-L. Lee, "Strain engineering for the solution of efficiency droop in InGaN/GaN light-emitting diodes," Optics express, vol. 18, no. 6, pp. 5466-5471, 2010.

[48] D.-J. Kong, S.-Y. Bae, C.-M. Kang, and D.-S. Lee, "InGaN/GaN microcolumn light-emitting diode arrays with sidewall metal contact," Optics express, vol. 21, no. 19, pp. 22320-22326, 2013.

[49] Y.-H. Ra, R. Navamathavan, H.-I. Yoo, and C.-R. Lee, "Single Nanowire Light-

Emitting Diodes Using Uniaxial and Coaxial InGaN/GaN Multiple Quantum Wells Synthesized by Metalorganic Chemical Vapor Deposition," Nano letters, 2014.

[50] Q. Wang, J. Bai, Y. Gong, and T. Wang, "Influence of strain relaxation on the optical properties of InGaN/GaN multiple quantum well nanorods," Journal of Physics D: Applied Physics, vol. 44, no. 39, p. 395102, 2011.

[51] S.-I. Na, H. Ga-Young, H. Dae-Seob, K. Seok-Soon, J.-Y. Kim, L. Jae-Hong, et al., "Selective wet etching of p-GaN for efficient GaN-based light-emitting diodes," Photonics Technology Letters, IEEE, vol. 18, no. 14, pp. 1512-1514, 2006.

초 록

질화갈륨 발광다이오드의 재결합 상수들과 내부 양자 효율을 추출하기 위해, 과도(transient) 특성을 이용한 빠르고 신뢰성 있는 측정 방법을 개발하였다. 또한 재결합 상수와 내부 양자 효율의 보다 정확한 측정을 위해, 발광 영역(active region)의 실질적인 부피를 고려한 질화갈륨 발광다이오드의 보다 개선된 반응 모델을 제안하였다. TCAD 시뮬레이션 연구를 통해 내부 양자 효율, 특히 'effciency droop' 현상이 실질적인 발광 영역의 감소와 관련되어 있는 것을 확인하였다. 또한 이러한 발광 영역의 감소가 극성 전하(polarization charge), 양자 우물 간의 장벽, 전류 밀도에 의해 결정되는 것을 확인하였다.

질화갈륨 발광다이오드의 트랩(trap)과 그 영향에 대해서도 측정과 TCAD 시뮬레이션을 통해 분석하였다. 질화갈륨 소자에 일정한 전압을 인가하였을 때, 회복 가능한 전류의 증가가 나타남을 확인하였으며, 이러한 현상은 트랩에 의해 나타나는 현상으로 생각되며 이 때, 트랩의 활성화 에너지(activation energy)가 0.30 eV 임을 추출하였다. TCAD 시뮬레이션을 통해 정공이 이 트랩에 갇히면서 양자 우물 간의 장벽의 높이가 감소하고 그에 따라 전류가 증가하는 현상이 나타남을 확인하였다. 또한, 이러한 트랩이 발광 소자의 광학적 특성과 신뢰성에 미치는 영향을 TCAD 시뮬레이션과 측정을 통해 확인하였다.

질화갈륨 발광다이오드의 내부 양자 효율 향상을 위해, 다중 양자 우물 내에 p-type trench를 삽입한 새로운 구조를 제안하였다. TCAD 시뮬레이션을 통해 p-type trench를 통해 정공이 다중 양자 우물 내에 효율적으로 주입되고, 그에 따라 제안한 구조의 다중 양자 우물 내의 정공의 분포가 훨씬 더 균일해짐을 확인하였다. 또한 CL 측정을 통해 제안한 구조가 strain relaxation과 QCSE의 감소에도 상당한 효과가 있음을 확인하였다. 더불어, 제안한 구조를 제작하기 위해 e-beam lithography, 또는 selective wet etching을 활용한 간단한 공정 방법을 제시하였다. 제작된 소자의 측정을 통해, e-beam lithography나 selective wet etching을 통해 제작한 소자에서 기존 소자에 비해 균일한 정공 분포와 strain의 감소로 광 출력이 크게 향상됨을 확인하였다.

본 연구를 통해 질화갈륨 발광다이오드의 내부 양자 효율과 이를 제한하는 요소들을 분석할 수 있는 방법들을 제시하였다. 또한 다중 양자 우물 내에 p-type trench를 삽입한 구조가 질화갈륨 발광다이오드의 ‘efficiency droop’ 문제 해결에 강력한 후보가 될 수 있음을 검증했다.

주요어: 질화갈륨 발광 소자, 내부 양자 효율, efficiency droop, 전류 과도 특성 분석, p-type trench 구조

학 번: 2008-20829

List of Publications

International Journal

[1] **Garam Kim**, Sang Wan Kim, Jang Hyun Kim, Euyhwan Park, and Byung-Gook Park, " Effects of periodic trench structure on the cathodo-luminescence in InGaN/GaN multi-quantum-wells," Electronics Letters, Vol. 50, No. 14, pp. 1012-1014, Jul. 2014

[2] **Garam Kim**, Euyhwan Park, Jang Hyun Kim, Jong-Ho Bae, Dong hoon Kang, and Byung-Gook Park, "Analysis of trap and its impact on InGaN-based blue light-emitting diodes using current-transient methodology," Japanese Journal of Applied Physics: Regular Papers, Vol. 53, No. 6, pp. 062101-1-062101-5, May. 2014 [SCI]

[3] **Garam Kim**, Jang Hyun Kim, Euyhwan Park, Donghoon-Kang, and Byung-Gook Park, "Improved internal quantum efficiency of GaN-based light emitting diodes using p-AlGaN trench in multi-quantum well," Japanese Journal of Applied Physics: Regular Papers, Vol. 53, No. 6S, pp. 06JE14-1-06JE14-4, May. 2014 [SCI]

[4] **Garam Kim**, Jang Hyun Kim, Euyhwan Park, Donghoon Kang, and Byung-Gook Park, "Extraction of recombination coefficients and internal quantum efficiency of GaN-based light emitting diodes considering effective volume of active region," Optics Express, Vol. 22, No. 2, pp. 1235-1242, Jan. 2014 [SCI]

[5] Min-Chul Sun, **Garam Kim**, Jung Han Lee, Hyungjin Kim, Sang Wan Kim, Hyun Woo Kim, Jong-Ho Lee, Hyungcheol Shin, and Byung-Gook Park, "Patterning of Si nanowire array with electron beam lithography for sub-22 nm Si nanoelectronics technology," Microelectronic Engineering, Vol. 110, No. , pp. 141-146, Oct. 2013 [SCI]

[6] Jang Hyun Kim, **Garam Kim**, Euyhwan Park, and Byung-Gook Park, "Analysis of the internal quantum efficiency of gallium-nitride-based light-emitting diodes from the transient electro-luminescence characteristics," Journal of the Korean Physical Society, Vol. 63, No. 3, pp. 1186-1188, Sep. 2013 [SCI]

[7] Euyhwan Park, **Garam Kim**, Wandong Kim, Jang Hyun Kim, Donghoon Kang, Joong-Kon Son, and Byung-Gook Park, "Enhancement of radiative recombination by different indium composition of multiple quantum barriers in GaN-based light-emitting diodes," Japanese Journal of Applied Physics: Regular Papers, Vol. 52, No. , pp. 06GE04-1-06GE04-5, Jun. 2013 [SCI]

[8] Min-Chul Sun, Sang Wan Kim, **Garam Kim**, Hyun Woo Kim, Hyungjin Kim, and Byung-Gook Park, "Novel tunneling field-effect transistor with sigma-shape embedded SiGe sources and recessed channel," IEICE Transactions on Electronics, Vol. E96-C, No. 5, pp. 639-643, May. 2013 [SCIE]

[9] Hyun Woo Kim, Jang Hyun Kim, Sang Wan Kim, Min-Chul Sun, **Garam Kim**, Euyhwan Park, Hyungjin Kim, Kyung Wan Kim, and Byung-Gook Park, "A novel fabrication method for the nanoscale tunneling field effect transistor," Journal of Nanoscience and Nanotechnology, Vol. 12, No. 5, pp. 5592-5597, Jul. 2012 [SCI]

[10] Min-Chul Sun, **Garam Kim**, Sang Wan Kim, Hyun Woo Kim, Hyungjin Kim, Jong-Ho Lee, Hyungcheol Shin, and Byung-Gook Park, "Co-Integration of nano-scale vertical- and horizontal-channel metal-oxide-semiconductor field-effect transistors for low power CMOS technology," Journal of Nanoscience and Nanotechnology, Vol. 12, No. 7, pp. 5313-5317, Jul. 2012 [SCI]

[11] Min-Chul Sun, Hyun Woo Kim, Sang Wan Kim, **Garam Kim**, Hyungjin Kim, and Byung-Gook Park, "Comparative study on top- and bottom-source vertical-channel tunnel field-effect transistors," IEICE Transactions on Electronics, Vol. E95-C, No. 5, pp. 826-830, May. 2012 [SCIE]

[12] Hyungjin Kim, Min-Chul Sun, Hyun Woo Kim, Sang Wan Kim, **Garam Kim**, and Byung-Gook Park, "Study on threshold voltage control of tunnel field-effect transistors using VT-control doping region," IEICE Transactions on Electronics, Vol. E95-C, No. 5, pp. 820-825, May. 2012 [SCIE]

[13] Min-Chul Sun, Sang Wan Kim, Hyun Woo Kim, **Garam Kim**, Hyungjin Kim, Jong-Ho Lee, Hyungcheol Shin, and Byung-Gook Park, "Design of thin-body double-gated vertical-channel tunneling field-effect transistors for ultralow-power logic circuits," Japanese Journal of Applied Physics: Regular Papers, Vol. 51, No. 4, pp. 04DC03-1-04DC03-5, Apr. 2012 [SCI]

[14] Seongjae Cho, Min-Chul Sun, **Garam Kim**, Theodore I. Kamins, Byung-Gook Park, and James S. Harris, Jr., "Design Optimization of a Type-I Heterojunction Tunneling Field-Effect Transistor (I-HTFET) for High Performance Logic Technology," Journal of Semiconductor Technology and Science, Vol. 11, No. 3, pp. 182-189, Sep. 2011 [SCIE]

[15] **Garam Kim**, Sang Wan Kim, Kyung-Chang Ryoo, Jeong-Hoon Oh, Min-Chul Sun, Hyun Woo Kim, Dae Woong Kwon, Jisoo Chang, Sunghun Jung, and Byung-Gook Park, "Split-Gate-Structure 1T DRAM for Retention Characteristic Improvement," Journal of Nanoscience and Nanotechnology, Vol. 11, No. 7, pp. 5603-5607, Jul. 2011 [SCI]

[16] Taewook Kang, Jungjin Park, Jung-Kyu Lee, **Garam Kim**, Daeyoung Woo, Joong Kon Son, Jong-Ho Lee, Byung-Gook Park, and Hyungcheol Shin, "Random telegraph noise in GaN-based light-emitting diodes," Electronics Letters, Vol. 47, No. 15, pp. 1-2, Jul. 2011

[17] Joung-Eob Lee, **Garam Kim**, Kyung Wan Kim, Jung-Han Lee, Kwon-Chil Kang, Jong-Ho Lee, Hyungcheol Shin, and Byung-Gook Park, "Dynamic Driving Current Using Side Gate Bias of Single-Electron Transistors," Japanese Journal of Applied Physics: Regular Papers, Vol. 50, No. 7, pp. 074101-1-074101-5, Jul. 2011 [SCI]

[18] Jang-Gn Yun, **Garam Kim**, Joung-Eob Lee, Yoon Kim, Won Bo Shim, Jong-Ho Lee, Hyungcheol Shin, Jong Duk Lee, and Byung-Gook Park, "Single-Crystalline Si STacked ARray (STAR) NAND flash memory," IEEE Transactions on Electron Devices, Vol. 58, No. 4, pp. 1006-1014, Apr. 2011 [SCI]

[19] Dae Woong Kwon, Jang Hyun Kim, Jisoo Chang, Sang Wan Kim, Min-Chul Sun, **Garam Kim**, Hyun Woo Kim, Jae Chul Park, Ihun Song, Chang Jung Kim, U In Jung, and Byung-Gook Park, "Charge injection from gate electrode by simultaneous stress of optical and electrical biases in HfInZnO amorphous oxide thin film transistor," Applied Physics Letters, Vol. 97, No. 19, pp. 1935041-1935043, Nov. 2010 [SCI]

[20] Joung-Eob Lee, **Garam Kim**, Jang-Gn Yun, Kwon-Chil Kang, Jung Han Lee, Dae-Hwan Kim, Jong-Ho Lee, Hyungcheol Shin, and Byung-Gook Park, "Dual Gate Single-Electron Transistors with a Recessed Channel and Underlapped Source/Drain Structure," Japanese Journal of Applied Physics: Regular Papers, Vol. 49, No. 11, pp. 1152011-1152015, Nov. 2010 [SCI]

[21] Joung-Eob Lee, **Garam Kim**, Kyung Wan Kim, Won Bo Shim, Jung Han Lee, Kwon-Chil Kang, Jang-Gn Yun, Jong-Ho Lee, Hyungcheol Shin, and Byung-Gook Park, "Room-Temperature Operation of a Single-Electron Transistor Made by Oxidation Pocess Using the Recessed Channel Structure," Japanese Journal of Applied Physics: Regular Papers, Vol. 49, No. 11, pp. 1152021-1152026, Nov. 2010 [SCI]

[22] Jae Young Song, Jong Pil Kim, Sang Wan Kim, Jeong-Hoon Oh, Kyung-Chang Ryoo, Min-Chul Sun, **Garam Kim**, Jang-Gn Yun, Hyungcheol Shin, and Byung-Gook Park, "Fin and recess-channel metal oxide semiconductor field effect transistor for sub-50nm dynamic random access memory cell," Japanese Journal of Applied Physics: Regular Papers, Vol. 49, No. 10, pp. 1042021-1042025, Oct. 2010 [SCI]

International Conference

[1] Jang Hyun Kim, **Garam Kim**, Joong Kon Song, Dong Hoon kang, and Byung-Gook Park, "Effects of current spreading in GaN-based light-emitting diodes using ITO spreading pillar," International Microprocesses and Nanotechnology Conference, pp. 7P-7-46-, Nov. 2013

[2] **Garam Kim**, Jang Hyun Kim, Euyhwan Park, Donghoon Kang, and Byung-Gook Park,

"Improved internal quantum efficiency of GaN-based light emitting diodes using p-AlGaN trench in multi-quantum well," International Microprocesses and Nanotechnology Conference, pp. 7B-4-6-, Nov. 2013.
[3] **Garam Kim**, Euyhwan Park, Jang Hyun Kim, Jong-Ho Bae, Dong Hoon Kang, and Byung-Gook Park, "Trap analysis of InGaN-based blue light emitting diodes using current-transient methodology," International Conference on Solid State Devices and Materials, pp. 1000-1001, Sep. 2013
[4] Euyhwan Park, **Garam Kim**, Jang Hyun Kim, Donghoon Kang, Joong-Kon Son, and Byung-Gook Park, "Various size images mapping technique to analyze trap-assisted non-radiative recombination mechanism using cathodo- and electro- luminescenes measurement in GaN-based LEDs," IEEE International NanoElectronics Conference, pp. 112-114, Jan. 2013.
[5] Hyun Woo Kim, Min-Chul Sun, Sang Wan Kim, Joo Yun Seo, **Garam Kim**, Jang Hyun Kim, and Byung-Gook Park, "Investigation on effects of changing body doping concentration in short-channel junctionless transistor," International Microprocesses and Nanotechnology Conference, pp. 1P-7-41-, Nov. 2012
[6] Min-Chul Sun, **Sang Wan Kim**, Hyun Woo Kim, Hyungjin Kim, and Byung-Gook Park, "CMOS-compatible tunnel FETs with 14 nm gate, sigma-shape source, and recessed channel," *International Microprocesses and Nanotechnology Conference (MNC)*, Sapporo, Japan, pp. 1P-7-34-, Nov. 4-7, 2012.
[7] Euyhwan Park, **Garam Kim**, Wandong Kim, Jang Hyun Kim, Donghoon Kang, Joong-Kon Son, and Byung-Gook Park, "Radiative recombination enhancement by different indium composition multiple quantum barriers in GaN based LEDs," International Microprocesses and Nanotechnology Conference, pp. 11P-11-25-, Nov. 2012
[8] Min-Chul Sun, **Garam Kim**, Jung Han Lee, Hyungjin Kim, Sang Wan Kim, Hyun Woo Kim, Jong-Ho Lee, Hyungcheol Shin, and Byung-Gook Park, "Patterning of Si nanowire array with electron beam lithography for Sub-22nm Si Nanoelectronics Technology," International Conference on Micro- and Nano-Engineering, pp. 281-, Sep. 2012
[9] Hyungjin Kim, Jung Han Lee, **Garam Kim**, Min-Chul Sun, and Byung-Gook Park, "Silicon-based floating-body synaptic transistor," International Conference on Solid State Devices and Materials, pp. 322-323, Sep. 2012
[10] Euyhwan Park, **Garam Kim**, Jang Hyun Kim, Donghoon Kang, Joong-Kon Son, and Byung-Gook Park, "Cathodo- and electro- luminescences image mapping technique to study traps in GaN-based LEDs," IEEE NANO, pp. 7577-, Aug. 2012
[11] Min-Chul Sun, Sang Wan Kim, **Garam Kim**, Hyun Woo Kim, Hyungjin Kim, Jong-Ho Lee, Hyungcheol Shin, and Byung-Gook Park, "Novel tunneling field-effect transistor with sigma-shape embedded SiGe sources and recessed channel," Asia-Pacific Workshop on Fundamentals and Applications of Advanced Semiconductor Devieces, pp. 281-282, Jun. 2012
[12] Euyhwan Park, **Garam Kim**, Jang Hyun Kim, Donghoon Kang, Joong-Kon Son, and Byung-Gook Park, "Analysis of Non-radiative Recombination Mechanism Using Cathodoluminescence Measurement in GaN-based Light Emitting Diodes," International Conference on Electronics, Information and Communication, pp. 460-461, Feb. 2012
[13] Hyungjin Kim, Sang Wan Kim, Min-Chul Sun, Hyun Woo Kim, **Garam Kim**, Jang Hyun Kim, Euyhwan Park, and Byung-Gook Park, "Enhanced Ambipolar Characteristic of Tunneling Field-Effect Transistors Using Doped Region," International Conference on Electronics, Information and Communication, pp. 279-280, Feb. 2012
[14] Hyun Woo Kim, Jung Han Lee, Wandong Kim, Min-Chul Sun, Jang Hyun Kim, **Garam Kim**, Kyung Wan Kim, Hyungjin Kim, Joo Yun Seo, and Byung-Gook Park, "A Tunneling Field-Effect Transistor using Side Metal Gate/High-k material for Low Power Application," International Semiconductor Device Research Symposium, pp. 1-2, Dec. 2011.
[15] Min-Chul Sun, Sang Wan Kim, **Garam Kim**, Hyun Woo Kim, Hyungjin Kim, Jong-Ho Lee, Hyungcheol Shin, and Byung-Gook Park, "Modulation of Transfer Characteristics of Si Nanowire Tunnel FET on Ultra-Thin-Body and BOX (UTBB) SOI Substrate Using Back-Gate Bias," International Semiconductor Device Research Symposium, pp. 1-2, Dec. 2011
[16] **Garam Kim**, Min-Chul Sun, Sang Wan Kim, Hyun Woo Kim, Jang Hyun Kim, Euyhwan

Park, Hyungjin Kim, and Byung-Gook Park, "Novel MOSFET Structure using p-n Junction Gate for Ultra-low Subthreshold-Swing," International Semiconductor Device Research Symposium, pp. 1-2, Dec. 2011
[17] Min-Chul Sun, Sang Wan Kim, Hyun Woo Kim, **Garam Kim**, Hyungjin Kim, Jong-Ho Lee, Hyungcheol Shin, and Byung-Gook Park, "Design of Thin-Body Double-Gated Vertical-Channel Tunneling Field-Effect Transistors for Ultra-Low Power Logic Circuits," International Conference on Solid State Devices and Materials, pp. 845-846, Sep. 2011.
[18] Seongjae Cho, Min-Chul Sun, **Garam Kim**, Byung-Gook Park, and James S. Harris, "Design Optimization of Type-I Heterojunction Tunneling Field-Effect Transistor (I-HTFET) of Ge-AlxGa1-xAs System for High Performance Logic Technology," International Technical Conference on Circuits/Systems, Computers and Communications, pp. 312-313, Jun. 2011
[19] **Garam Kim**, Sang Wan Kim, Min-Chul Sun, Hyun Woo Kim, Hyungjin Kim, and Byung-Gook Park, "Tunneling Field Effect Transistor with Sidewall Floating Gate for Ultra-Low Subthreshold Swing," International Technical Conference on Circuits/Systems, Computers and Communications, pp. 306-307, Jun. 2011.
[20] Min-Chul Sun, Hyun Woo Kim, Sang Wan Kim, **Garam Kim**, Hyungjin Kim, Jong-Ho Lee, Hyungcheol Shin, and Byung-Gook Park, "Comparative Study on Top- and Bottom-Source Vertical-Channel Tunnel Field-Effect Transistors," Asia-Pacific Workshop on Fundamental and Application of Advanced Semiconductor Devices, pp. 87-89, Jun. 2011
[21] Hyungjin Kim, Min-Chul Sun, Hyun Woo Kim, Sang Wan Kim, **Garam Kim**, Jong-Ho Lee, Hyungcheol Shin, and Byung-Gook Park, "Threshold Voltage Control of Tunnel Field-Effect Transistors Using VT-control Doping Region," Asia-Pacific Workshop on Fundamental and Application of Advanced Semiconductor Devices, pp. 90-92, Jun. 2011
[22] Min-Chul Sun, Sang Wan Kim, **Garam Kim**, Hyun Woo Kim, Jong-Ho Lee, Hyungcheol Shin, and Byung-Gook Park, "Scalable Embedded Ge-Junction Vertical-Channel Tunneling Field-Effect Transistor for Low-Voltage Operation," IEEE Nanotechnology Materials and Devices Conference, pp. 286-290, Oct. 2010
[23] Min-Chul Sun, Wandong Kim, Jeong-Hoon Oh, Kyung-Chang Ryoo, Sang Wan Kim, **Garam Kim**, Hyun Woo Kim, Sunghun Jung, Dae Woong Kwon, Jisoo Chang, Jang Hyun Kim, and Byung-Gook Park, "Influence of Sidewall Thickness Variation on Transfer Characteristics of L-shaped Impact-Ionization MOS Transistor," IEEE NANO, pp. 1009-1009, Aug. 2010
[24] Sang Wan Kim, **Garam Kim**, Won Bo Shim, Jong-Ho Lee, Hyungcheol Shin, and Byung-Gook Park, "Simulation of Retention Characteristics in a Double-Gate and Recessed-Channel 1T DRAM cell with High Reliability," ITC-CSCC, pp. 905-906, Jul. 2010
[25] Kyung-Chang Ryoo, Jeong-Hoon Oh, Sunghun Jung, Sang Wan Kim, Min-Chul Sun, **Garam Kim**, Hyun Woo Kim, Dae Woong Kwon, Jisoo Chang, Jang Hyun Kim, Hongsik Jeong, and Byung-Gook Park, "Relationships of Resistive Switching Parameters of Resistive Random Access Memory (RRAM) for High Density and Low Power Application," International Conference on Electronics, Information and Communication(ICEIC), pp. 11-13, Jun. 2010
[26] Sang Wan Kim, **Garam Kim**, Wonjoo Kim, Hyoungsoo Ko, and Byung-Gook Park, "Investigation of 1T DRAM Cell with Non-Overlap Structure and Recessed Channel," Silicon Nanoelectronics Workshop, pp. 139-140, Jun. 2010
[27] Jae Young Song, Jong Pil Kim, Sang Wan Kim, Jeong-Hoon Oh, Kyung-Chang Ryoo, Min-Chul Sun, **Garam Kim**, Hyun Woo Kim, Jisoo Chang, Sunghun Jung, Hyungcheol Shin, and Byung-Gook Park, "Fabrication and Characterization of Buried-Gate Fin and Recess Channel MOSFET for High Performance and Low GIDL Current", 2009 International Semiconductor Device Research Symposium, Baltimore, USA, Dec. 9-11, 2009.
[28] Jae Young Song, Jong Pil Kim, Sang Wan Kim, Jeong-Hoon Oh, Kyung-Chang Ryoo, Jae Hyun Park, **Garam Kim**, Hyun Woo Kim, Atteq Ur Rehman, Jong Duk Lee, Hyungcheol Shin, and Byung-Gook Park, "Buried-Gate Fin and Recess Channel MOSFET for Sub-30 nm DRAM Cell Transistors with High Performance and Low GIDL Current", 2009 Silicon Nanoelectronics Workshop, Kyoto, Japan, pp. 51-52, June 13-14, 2009.
[29] **Garam Kim,** Sang Wan Kim, Jae Young Song, Jong Pil Kim, Kyung-Chang Ryoo, Jeong-

Hoon Oh, Jae Hyun Park, Hyun Woo Kim and Byung-Gook Park, "Body-Raised Double-Gate Structure for 1T DRAM", 2009 IEEE Nanotechnology Materilas and Devices Conference, Traverse City, Michigan, USA, pp.259-263, June 2-5, 2009.

Domestic Conference

[1] **Garam Kim,** Jang Hyun Kim, Euyhwan Park, and Byung-Gook Park, "Current crowding improvement of InGaN-based blue light-emitting diodes by modifying metal contact geometry," Korean Conference on Semiconductors, pp. 355-355, Feb. 2014

[2] Hyun Woo Kim, Jong Pil Kim, Sang Wan Kim, Min-Chul Sun, **Garam Kim**, Jang Hyun Kim, Euyhwan Park, and Byung-Gook Park, "Schottky barrier tunneling field-effect transistor using spacer technique," Korean Conference on Semiconductors, pp. 294-294, Feb. 2014

[3] Euyhwan Park, **Garam Kim**, Jang Hyun Kim, Sang Wan Kim, Joong-Kon Son, Donghoon Kang, and Byung-Gook Park, "GaN 발광 다이오드의 ITO층 습식식각 공정에 따른 cathodoluminescene 이미지 분석," 하계종합학술대회, pp. 77-78, Jun. 2012.

[4] **Garam Kim**, Jang Hyun Kim, Euyhwan Park, Joong-Kon Son, Donghoon Kang, Hyungcheol Shin, and Byung-Gook Park, "비정상적인 I-V 특성을 보이는 GaN LED 소자에 대한 전기적, 광학적 분석," 하계종합학술대회, pp. 144-145, Jun. 2012

[5] Min-Chul Sun, Hyungjin Kim, Sang Wan Kim, **Garam Kim**, Hyun Woo Kim, Jong-Ho Lee, Hyungcheol Shin, and Byung-Gook Park, "Ground-Plane Doping for VT-modulation of Planar Tunnel Field-Effect Transistors on Ultra-Thin-Body and BOX (UTBB) SOI Substrate," Korean Conference on Semiconductors, pp. 123-124, Feb. 2012

[6] Hyun Woo Kim, Hyungjin Kim, Sang Wan Kim, Min-Chul Sun, **Garam Kim**, Euyhwan Park, Jang Hyun Kim, and Byung-Gook Park, "A Novel Fabrication Method for Nanoscale Tunneling Field-Effect Transistor," NANO Korea, pp. O1102_006-O1102_006, Aug. 2011

[7] Min-Chul Sun, **Garam Kim**, Sang Wan Kim, Hyun Woo Kim, Hyungjin Kim, Jong-Ho Lee, Hyungcheol Shin, and Byung-Gook Park, "Co-Integration of Nano-scale Vertical- and Horizontal-Channel MOSFETs for Low Power CMOS Technology," NANO Korea, pp. O1101_010-O1101_010, Aug. 2011

[8] **Garam Kim**, Jang Hyun Kim, Euyhwan Park, Joong-Kon Son, Daeyoung Woo, Sang Wan Kim, Min-Chul Sun, Hyun Woo Kim, and Byung-Gook Park, "Optical and Electrical Degradation of GaN LED by Thermal stress," NANO Korea, pp. P1101_178-P1101_178, Aug. 2011

[9] Euyhwan Park, **Garam Kim**, Jang Hyun Kim, Sang Wan Kim, Joong-Kon Son, Daeyoung Woo, Jong-Ho Lee, Hyungcheol Shin, and Byung-Gook Park, "GaN 발광 다이오드의 전류 포화 지연현상 분석," 하계종합학술대회, pp. 461-462, Jun. 2011

[10] Hyun Woo Kim, Sang Wan Kim, Min-Chul Sun, **Garam Kim**, Dae Woong Kwon, Jisoo Chang, Jang Hyun Kim, Euyhwan Park, and Byung-Gook Park, "터널링 전계효과 트랜지스터의 양극성 현상을 줄이기 위한 공정 방법," 대한전자공학회 추계학술대회, pp. 46-47, Nov. 2010

[11] **Garam Kim**, Sang Wan Kim, Kyung-Chang Ryoo, Jeong-Hoon Oh, Min-Chul Sun, Hyun Woo Kim, Dae Woong Kwon, Jisoo Chang, Sunghun Jung, Jang Hyun Kim, and Byung-Gook Park, "Split gate structure 1T DRAM for improving retention characteristics," NANO Korea, pp. 1034-1034, Aug. 2010

[12] Sang Wan Kim, **Garam Kim**, Won Bo Shim, Min-Chul Sun, Hyun Woo Kim, Dae Woong Kwon, Jisoo Chang, Jang Hyun Kim, Euyhwan Park, Jong-Ho Lee, Hyungcheol Shin, and Byung-Gook Park, "1T DRAM Cell with Twin Gates and Recessed Channel," 하계 종합 학술발표회 논문집, pp. 723-724, Jun. 2010

[13] Min-Chul Sun, Sang Wan Kim, **Garam Kim**, Hyun Woo Kim, Jong-Ho Lee, Hyungcheol Shin, and Byung-Gook Park, "Short-Channel Characteristics of Tunneling Field-Effect Transistor and Operation of Vertical-Channel Tunneling Field-Effect Transistor," 하계 종합 학술발표회 논문집, pp. 727-729, Jun. 2010

[14] Jang-Gn Yun, Seongjae Cho, Jung Hoon Lee, Gil Sung Lee, Yoon Kim, Dong Hua Li, Se Hwan Park, Won Bo Shim, **Garam Kim**, and Byung-Gook Park, "Three Dimensional Stacked Bit-line NAND Flash Array and Inter-layer Interference," Korean Conference on

Semiconductors, pp. 53-54, Feb. 2010

Patents

[1] 박병국, 김형진, 김가람, 이정한, 권민우, “시냅스 모방 반도체 소자 및 그 동작방법,”
· Korean Patent filed 10-2012-0098767, September 6, 2012
· United States Patent filed 14/018693, September 5, 2013
[2] 박병국, 김장현, 김가람, 박의환, 강동훈, 손중곤, “반도체 발광소자,”
· Korean patent filed 10-2012-0142998,
[3] 박병국, 김가람, “스플릿게이트 구조를 갖는 1T 디램 소자 및 이를 이용한 디램 어레이,”
· Korean patent filed 10-2010-0056777, June 15, 2010
· Korean patent No.1147523, May 11, 2012
[4] 박병국, 김가람, “2비트 저장 가능한 단일 트랜지스터 구조를 갖는 디램 소자,”
· Korean patent filed 10-2010-0129644, December 17, 2010
· Korean patent No.1091010, December 1, 2011
[5] 박병국, 김가람, “돌출된 바디를 저장노드로 하는 메모리 셀 및 그 제조방법,”
· Korean Patent filed 10-2009-0049080, June 3, 2009
· Korean Patent No.1089659, November 29, 2011